

# The Transcription Regulator RcoM-2 from *Burkholderia xenovorans* Is a Cysteine-Ligated Hemoprotein That Undergoes a Redox-Mediated Ligand Switch<sup>†</sup>

Katherine A. Marvin,<sup>‡</sup> Robert L. Kerby,<sup>§</sup> Hwan Youn,<sup>§</sup> Gary P. Roberts,<sup>§</sup> and Judith N. Burstyn<sup>\*‡</sup>

Department of Chemistry, University of Wisconsin, 1101 University Avenue, and Department of Bacteriology, University of Wisconsin, 1550 Linden Drive, Madison, Wisconsin 53706

Received March 20, 2008; Revised Manuscript Received June 24, 2008

**ABSTRACT:** Spectroscopic characterization of the newly discovered heme-PAS domain sensor protein BxRcoM-2 reveals that this protein undergoes redox-dependent ligand switching and CO- and NO-induced ligand displacement. The aerobic bacterium *Burkholderia xenovorans* expresses two homologous heme-containing proteins that promote CO-dependent transcription in vivo. These regulators of CO metabolism, BxRcoM-1 and BxRcoM-2, are gas-responsive heme-PAS domain proteins like mammalian neuronal PAS domain protein 2 (NPAS2) and the direct oxygen sensor from *Escherichia coli* (EcDos). BxRcoM-2 was studied using electronic absorption, MCD, resonance Raman, and EPR spectroscopies. In the Fe(III) oxidation state, the heme is low-spin and six-coordinate with a cysteine(thiolate) as one of the two ligands. The sixth ligand is a histidine (His<sup>74</sup>), which is present in all states of the protein that were studied. Reduction to the Fe(II) oxidation state results in replacement of the cysteine(thiolate) with a neutral thioether ligand, Met<sup>104</sup>. CO and NO bind to the Fe(II)BxRcoM-2 heme opposite the histidine ligand. Thus, BxRcoM-2 employs coordination state changes similar to those known for CO-sensing CooA, with redox-dependent loss of a cysteine(thiolate) ligand and displacement of a relatively weakly bound axial ligand by the effector gas molecule. Like EcDos, the weakly bound axial ligand that is displaced is methionine.

The past decade has witnessed the discovery of many new heme-containing gas-sensing proteins, which couple the binding of diatomic ligands at a heme center to the regulation of protein function. Binding of O<sub>2</sub>, CO, or NO effector molecules to heme iron acts as a switch for an allosteric conformational change; the environment of the heme pocket often discriminates against functional activation by more than

one specific ligand (1, 2). Oxygen sensors include bacterial FixL<sup>1</sup> (3), EcDos (4), and HemAT (5); the CO sensors include bacterial RrCooA (6) and mammalian NPAS2 (7), and the NO sensors include mammalian sGC (8) and bacterial H-NOX proteins (9). This diverse collection of proteins frequently utilizes a single-component signal transduction system with a heme-binding domain and a functional domain, which may be a guanylyl cyclase, phosphodiesterase, or DNA binding domain. We report herein spectroscopic characterization of a new protein of this class, BxRcoM-2, a putative regulator of aerobic CO metabolism.

A number of heme-based sensor proteins, including FixL, EcDos, and NPAS2, bind heme within a conserved PAS domain. PAS domains are found in proteins spanning all kingdoms of life (10). The basic domain structure is an a/b fold of ~130 amino acids, although the level of sequence identity among PAS-bearing proteins is quite low. Sensing environmental signals through small molecule binding is a function associated with PAS domains. Only a few PAS-containing proteins are known to bind cofactors such as FAD, FMN, and heme, and among these, the heme-containing PAS domain proteins are the best-characterized. The heme-PAS sensor kinase FixL is the regulator of a two-component signal transduction system, which phosphorylates the transcription factor FixJ (3, 11). Under aerobic conditions, binding of O<sub>2</sub> to the heme in FixL inhibits kinase activity. Release of O<sub>2</sub> from the heme under hypoxic conditions stimulates phosphorylation of FixJ, triggering a cascade that results in production of the nitrogen fixation machinery. CO and NO also inhibit the kinase activity of FixL, although with much

<sup>†</sup> This work was supported by NIH Grants HL-66147 (J.N.B.) and GM-53228 (G.P.R.).

\* To whom correspondence should be addressed. Telephone: (608) 262-0328. Fax: (608) 262-6143. E-mail: burstyn@chem.wisc.edu.

<sup>‡</sup> Department of Chemistry.

<sup>§</sup> Department of Bacteriology.

<sup>1</sup> Abbreviations: AxPDEA1, *Acetobacter xylinum* phosphodiesterase A1; BMAL1, brain and muscle Arnt-like protein 1; CCP, cytochrome c peroxidase; ChCooA, a CooA homologue from the thermophilic bacterium *Carboxydotherrmus hydrogenoformans*; CooA, heme-containing CO-sensing transcriptional factor in *Rhodospirillum rubrum*; CPO, chloroperoxidase; EcDos, direct oxygen sensor in *Escherichia coli*; EPPS, 3-[4-(2-hydroxyethyl)-1-piperazinyl]propanesulfonic acid; EPR, electronic paramagnetic resonance; FixL, O<sub>2</sub>-sensing heme protein that regulates expression of genes associated with N<sub>2</sub> fixation; hCBS, human cystathionine  $\beta$ -synthase, a heme-containing pyridoxal 5'-phosphate enzyme; HemAT, heme-based aerotactic transducer in *Bacillus subtilis*, an oxygen sensor; HRP, horseradish peroxidase; M80C cyt c, cytochrome c variant in which methionine is replaced with cysteine(thiolate) as an axial ligand to the Fe(III) heme; MCD, magnetic circular dichroism; MOPS, 3-(N-morpholino)propanesulfonic acid; NPAS2, neuronal PAS domain protein 2, a heme-containing CO-responsive eukaryotic transcriptional regulator; P450<sub>CAM</sub>, camphor-hydroxylating cytochrome P450 from *Pseudomonas putida*; P450<sub>CAM</sub>+ImH, P450<sub>CAM</sub> with imidazole as an axial ligand to the Fe(III) heme; PAS, domain structure named for the proteins in which the motif was first identified, Period, aryl hydrocarbon receptor nuclear translocator (ARNT), simple-minded proteins; RCCP, *Rhodobacter capsulatus* cytochrome c'; sGC, soluble guanylyl cyclase, an NO-sensing heme protein that catalyzes the conversion of GTP to cGMP.

reduced efficiencies (3- and 2-fold for CO and NO, respectively, vs 100-fold for O<sub>2</sub>) (12, 13).

The direct oxygen sensor in *E. coli* (EcDos) (4) and the *A. xylinum* phosphodiesterase A1 (AxPDEA1) (14) proteins are closely related to one another and to FixL, with PAS domains whose sequences are ~30% identical to that of FixL. These proteins combine an N-terminal PAS-fold heme domain with a phosphodiesterase enzymatic domain, a module found only in bacterial signal transduction systems. AxPDEA1 regulates cellulose synthase, which is allosterically activated by the precursor molecule 3',5'-cyclic diguanylic acid (c-di-GMP). Under aerobic conditions, AxPDEA1 is inhibited by O<sub>2</sub> binding to the PAS-domain heme. As oxygen tension decreases and O<sub>2</sub> is released, phosphodiesterase activity is stimulated, hydrolyzing c-di-GMP to the linear dinucleotide (pGpG) and inhibiting cellulose production. The sequence of EcDos is approximately 40% identical with AxPDEA1 over the heme and enzymatic domains (4). EcDos exhibits O<sub>2</sub>-dependent cAMP phosphodiesterase activity (15), as well as O<sub>2</sub>-, CO-, and NO-dependent c-di-GMP phosphodiesterase activity (16). Spectroscopic, structural, and mutagenesis studies indicate that EcDos is low-spin and six-coordinate in the Fe(III), Fe(II), and Fe(II) gas-bound states, and that signal transduction occurs via displacement of an endogenous ligand (Met<sup>95</sup>) (15–17).

PAS-domain heme-based sensor proteins are also known to bind to DNA and to function as transcriptional regulators. Neuronal PAS domain protein 2 (NPAS2) was the first eukaryotic heme-containing PAS-domain protein identified (7). NPAS2 is a transcription factor that binds to DNA as a heterodimer with BMAL1. NPAS2 is expressed in the central nervous system, where it regulates the expression of genes critical for controlling circadian rhythm (18). Each of the two PAS domains in NPAS2 contains a heme, and the binding of CO inhibits heterodimerization with BMAL1 and thus prevents transcription of NPAS2–BMAL1 regulated target genes (7).

CooA (CO oxidation activator) is a CO sensor from the bacterium *R. rubrum* and is the most thoroughly characterized heme-based sensor protein (6, 19). RrCooA, which does not contain a PAS domain, is a member of the cAMP receptor protein (CRP) family and fumarate and nitrate reductase (FNR) superfamily of transcriptional regulators. In the absence of oxygen, the specific binding of CO to the RrCooA heme activates transcription of the genes for the CO oxidation machinery, thus enabling *R. rubrum* to utilize CO as an energy source. The RrCooA homodimer consists of two domains: an N-terminal heme-binding regulatory domain and a C-terminal helix–turn–helix DNA-binding domain (20). The RrCooA dimer binds two *b*-type heme cofactors in the regulatory domain; the Fe(III) heme iron is coordinated by cysteine(thiolate) (Cys<sup>75</sup>) and by the nitrogen of the opposing monomer's N-terminal proline (Pro<sup>2</sup>) (21). When the heme is reduced, the cysteine(thiolate) is replaced with a neighboring histidine (His<sup>77</sup>) (22, 23), which poises the protein to bind CO via replacement of the coordinated proline. The binding of CO is proposed to trigger a global conformational change in which movement of the heme is translated through the dimer interface to the DNA binding domain (24, 25).

The newest members of the heme-based sensor family are heme-PAS transcription factors that may regulate aerobic CO

metabolism in bacteria. Two proteins were isolated from *Burkholderia xenovorans* (LB400) (26), an aerobic polychlorinated biphenyl (PCB)-degrading bacterium originally found in PCB-contaminated landfill sites in New York (27). Designated “regulators of CO metabolism” (RcoM), these two homologous proteins (BxRcoM-1 and BxRcoM-2, 88% identical and 93% similar in sequence) function as CO-dependent transcription factors in vivo (26). Each protein contains an N-terminal heme-containing PAS domain and a C-terminal LytTR DNA binding domain. The N-terminal PAS domain binds a *b*-type heme, and mutagenesis of two conserved residues, His<sup>74</sup> and Met<sup>104</sup> in BxRcoM-1, identified these residues as likely heme iron axial ligands.

Herein, we describe the spectroscopic characterization of the BxRcoM-2 protein in the Fe(III), Fe(II), Fe(II)CO, and Fe(II)NO states using the techniques of electronic absorption, magnetic circular dichroism, electron paramagnetic resonance, and resonance Raman spectroscopy. Our studies reveal that one of the two axial ligands in Fe(III)BxRcoM-2 is a cysteine(thiolate) that is replaced with a neighboring neutral residue, likely Met<sup>104</sup>, upon reduction of the heme iron. Binding of CO to the Fe(II) heme occurs opposite a neutral endogenous donor, likely His<sup>74</sup>, while NO binds with retention of a sixth nitrogen-containing ligand, presumably the same histidine. Drawing on our spectroscopic data, previous mutational analysis, and comparison to similar heme-containing PAS-domain proteins (26), we propose a model for heme coordination changes in BxRcoM-2 that are associated with redox and ligand binding events.

## MATERIALS AND METHODS

**Materials.** CO and NO gas (99.5%) cylinders were purchased from AGA, and <sup>13</sup>CO gas (99%) was purchased from Sigma-Aldrich. The NO gas was passed over an anaerobic KOH column to remove higher-order nitrogen oxides before use. Na<sup>15</sup>NO<sub>2</sub> (98%) was purchased from Cambridge Isotopes, while NaNO<sub>2</sub> was purchased from Fischer Scientific. Buffer and glycerol were purchased from Sigma-Aldrich; high-purity sodium dithionite was purchased from Fluka and stored under Ar(g) at –20 °C. All chemical reagents were used as received.

**Expression and Purification of BxRcoM-2.** The cloning, expression, and purification of the BxRcoM proteins have been described previously (26). In brief, the ~800 bp region encoding BxRcoM-2 was cloned into pEXT20 (28) with subsequent introduction of a segment that added a six-His tag at the C-terminus of the expressed protein. For expression, *E. coli* cultures were grown in rich medium supplemented with ferric citrate and IPTG, and the protein was purified as previously described (26). The purified protein was desalted by gel filtration into 25 mM MOPS (pH 7.4) and 500 mM KCl and stored at –80 °C. Protein concentrations were determined using the BCA method (Pierce, Rockford, IL) using bovine serum albumin as the standard, and heme content was determined using the pyridine heme-chrome assay (29). The protein purity was >90% as determined by SDS–PAGE analysis.

**Electronic Absorption Spectroscopy.** Electronic absorption spectra were recorded on a double-beam Varian Cary 4 Bio spectrophotometer equipped with a temperature controller and set to a spectral bandwidth of 0.5 nm. Spectra were obtained at 25 °C for protein samples diluted into 25 mM

EPPS and 500 mM KCl (pH 8.0). Protein solutions were purged with  $\text{Ar}_{(\text{g})}$  in the cuvette headspace to remove  $\text{O}_2$ . Reactions of the Fe(III) protein with a reducing agent (sodium dithionite,  $\text{Na}_2\text{S}_2\text{O}_4$ ) were performed anaerobically and were initiated by (1) the addition of an excess of the solid reductant under  $\text{Ar}_{(\text{g})}$  or (2) the addition of a stock solution of reductant, prepared anaerobically, to a final concentration of 2 mM. The specific method used is noted in individual figure legends. The Fe(II)CO adducts of BxRcoM-2 were generated by injection of  $\text{CO}_{(\text{g})}$  into the headspace of the septum-sealed cuvette via a gastight syringe, after which the solution was gently agitated.  $\text{CO}_{(\text{g})}$  was introduced either to the Fe(III) protein, followed by reduction, or to the prereduced Fe(II) protein for the observation of any order of addition effects. The Fe(II)NO adducts of BxRcoM-2 were generated by injection of  $\text{NO}_{(\text{g})}$  into the headspace of the septum-sealed cuvette via a gastight syringe, after which the solution of Fe(III)BxRcoM-2 or dithionite-reduced Fe(II)BxRcoM-2 was gently agitated. Typically, 50–200  $\mu\text{L}$  of  $\text{NO}_{(\text{g})}$  or  $\text{CO}_{(\text{g})}$  was used to form the NO and CO adducts; absorption spectra were recorded during the experiment at room temperature until no further changes were observed.

**MCD Spectroscopy.** Magnetic circular dichroism (MCD) spectra were recorded on a Jasco J-715 CD spectropolarimeter with the sample compartment modified to accommodate an Oxford Instruments SM-4000-8T magnetocryostat. MCD spectra were recorded at temperatures ranging from 2 to 100 K. The MCD signal at  $-7$  T for each temperature was subtracted from the  $+7$  T data, and the resulting trace was divided by 2 to remove the CD contribution to each spectrum. The buffer used for MCD samples consisted of 50 mM EPPS and 500 mM KCl (pH 8.0), with approximately 55% (v/v) glycerol present in the sample. Addition of glycerol had no effect on the visible absorption spectrum of any sample at room temperature, nor was any visible spectral change observed at temperatures at which MCD data were collected. Sodium dithionite was used as a reducing agent and was introduced in excess as a solid into anaerobic samples of the Fe(III) protein under  $\text{Ar}_{(\text{g})}$ . The CO adduct was prepared as noted for the absorption spectra. Each sample was transferred to an  $\text{Ar}_{(\text{g})}$ -filled cell via a gastight syringe and frozen in liquid nitrogen.

**EPR Spectroscopy.** X-Band EPR spectra were collected on a Bruker ESP 300E instrument equipped with an Oxford ESR 900 continuous-flow liquid helium cryostat and an Oxford ITC4 temperature controller. The microwave frequency was monitored using an EIP model 625A CW microwave frequency counter. Spectra were recorded at 10 K. Spectra of Fe(III)- and Fe(II)NO BxRcoM-2 (150  $\mu\text{L}$ ,  $\sim 250$   $\mu\text{M}$  heme) were recorded in 50 mM borate [ $\text{B}(\text{OH})_3$ ] buffer with additional 500 mM KCl at pH 8.0. For samples containing a reducing agent, sodium dithionite was added as a solid into anaerobic samples of the Fe(III) protein. The NO gas adducts were prepared using  $\text{Na}^{14}\text{NO}_2$  or  $\text{Na}^{15}\text{NO}_2$ ; NO gas was generated under anaerobic conditions in situ by the reduction of the appropriate  $\text{NaNO}_2$  reagent with a small excess of sodium dithionite in the aqueous protein solution. Each sample was then transferred to an  $\text{Ar}_{(\text{g})}$ -filled quartz EPR tube via a gastight syringe or  $\text{Ar}_{(\text{g})}$ -purged small-bore tubing and frozen in liquid nitrogen. For all samples, scans of 0–10000 G revealed no signals other than those

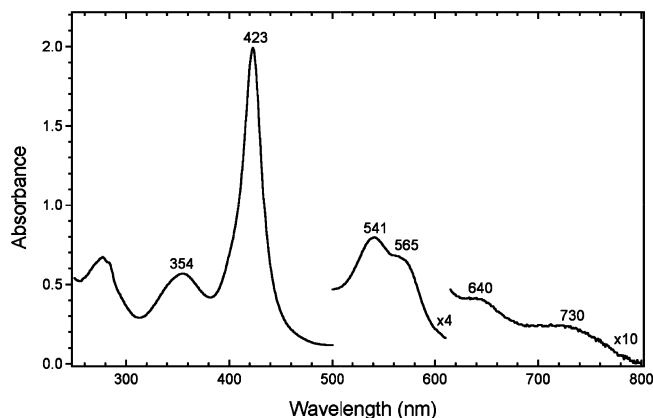


FIGURE 1: Electronic absorption spectrum of purified Fe(III)BxRcoM-2. The sample included 12  $\mu\text{M}$  heme in 25 mM EPPS buffer with 500 mM KCl (pH 8.0) at 25  $^{\circ}\text{C}$ .

reported. EPR data were simulated using the WEPR program written by F. Neese (30). The parameter set employed for the EPR simulation is given in the Supporting Information.

**Resonance Raman Spectroscopy.** Resonance Raman spectra were recorded with excitation wavelengths of 413.1 and 406.7 nm from a  $\text{Kr}^+$  laser (Coherent I-302C). The scattered light was collected using a back-scattering  $135^{\circ}$  sample geometry. Low incident laser powers of 50 mW for Fe(III) and Fe(II) states, or  $\sim 7$ –10 mW for CO and NO adducts to minimize photodissociation of ligands, were focused with a cylindrical lens onto the sample. An Acton Research triple monochromator equipped with 2400 grooves/mm gratings was used. Data were collected with a Princeton Instruments Spex 1877 triple spectrograph equipped with a cooled, intensified diode array detector. Data collection was automated using Spectrasense. Peak positions and intensities were calibrated using the ice peak at  $228\text{ cm}^{-1}$ . The frozen protein samples, in the same buffer that was used for EPR (vide infra), were placed in a quartz dewar and cooled to 77 K to reduce local heating. Windows centered at 650, 1250, and  $1850\text{ cm}^{-1}$  were collected to obtain a complete spectral window of  $\sim 150$ – $2250\text{ cm}^{-1}$ . All spectral data were imported into and processed with IGOR Pro (Wavemetrics, Inc.). Vibrational modes are indicated in the figures, with assignments based on comparison with those of other heme proteins and the work of Spiro and Kitagawa (31–34).

## RESULTS

**Characterization of Fe(III)BxRcoM-2.** The electronic absorption spectrum of Fe(III)BxRcoM-2 (Figure 1) exhibits optical features with similarities to those of known Fe(III) heme-thiolate proteins. The spectrum shown in Figure 1 is consistent with a low-spin, six-coordinate Fe(III) heme with an axial ligand environment consisting of a cysteine(thiolate) ligand opposite a neutral donor ligand, likely histidine. Key spectral characteristics are a  $\delta$  band at 354 nm, an intense Soret ( $\gamma$ ) peak at 423 nm, and broad, asymmetric  $\alpha$  and  $\beta$  features at 565 and 541 nm, respectively, and a pair of weak charge transfer bands at  $\sim 640$  and 730 nm. The two most significant optical features associated with coordination by cysteine(thiolate) include the  $\delta$  band in the near UV and charge transfer bands in the visible region (35). The  $\delta$  band is a feature associated with mixing of a sulfur-based ligand-to-metal charge transfer (LMCT) transition and the Fe(III)



Table 1: Comparison of Electronic Absorption Peak Positions for Low-Spin Six-Coordinate Fe(III) Heme Proteins

protein	ligands	$\delta$	Soret	$\beta$	$\alpha$	LMCT	ref
BxRcoM-2 <sup>a</sup>	?/Cys	354	423	541	565	640, 730	this work
RrCooA	Pro/Cys	362	424	540	574	649, 750	21
P450 <sub>CAM</sub> +ImH	ImH/Cys	358	425	542	574	638, 753	72
hCBS	His/Cys	365	428	550	NR	650, 700	56
M80C cyt <i>c</i>	His/Cys	355	416	540	570	635, 734	72
cytochrome <i>c</i>	His/Met		408	530	695		73
EcDos	His/H <sub>2</sub> O		416	530	564		74
cytochrome <i>b</i> <sub>5</sub>	His/His		413	532	566		75
neuroglobin	His/His		415	535	565		59

<sup>a</sup> Experimental values.

porphyrin ( $\pi \rightarrow \pi^*$ ) Soret transition. Additionally, when an Fe(III) heme is coordinated by a strong electron donor such as thiolate, the absorption spectrum exhibits two low-energy LMCT bands. Comparison of the spectral peak positions observed in Fe(III)BxRcoM-2 (Table 1) with those of other known heme-thiolate proteins, such as CooA from *R. rubrum*, cytochrome P450 with imidazole, and human cystathione  $\beta$ -synthase (hCBS), provides support for the assignment of Fe(III)BxRcoM-2 as another member of the class of low-spin six-coordinate heme-thiolate proteins.

The assignment of Fe(III)BxRcoM-2 as a low-spin, six-coordinate species is also supported by the MCD spectral features. The MCD spectrum of Fe(III)BxRcoM-2 shown in Figure S1 of the Supporting Information is dominated by an intense temperature-dependent, derivative-shaped *C* term in the Soret region with a crossover at 419 nm. Another temperature-dependent *C* term is also present in the  $\alpha$ – $\beta$  region with a crossover at 570 nm; the intensity of this term is much lower than that of the Soret feature. A magnetization plot ( $\Delta\epsilon$  vs  $\beta H/2kT$ ) of data for Fe(III)BxRcoM-2 (Supporting Information, Figure S1, inset) is consistent with a low-spin,  $S = 1/2$  heme. Comparison of the MCD peak positions of Fe(III)BxRcoM-2 (Supporting Information, Table S1) to those of other low-spin, six-coordinate Fe(III) heme proteins is consistent with the assignment of axial ligation by cysteine(thiolate) opposite a neutral donor such as histidine.

EPR, which is sensitive to the unpaired spin density on iron and the axial ligand environment, is clearly indicative of cysteine(thiolate) ligated to the Fe(III)BxRcoM-2 heme in a low-spin, six-coordinate system. The corrected and simulated spectra for Fe(III)BxRcoM-2 at pH 8.0 are depicted in Figure 2. The best-fit simulation yields *g* values of 1.88, 2.28, and 2.52 for  $g_x$ ,  $g_y$ , and  $g_z$ , respectively. Table 2 illustrates that these values are in agreement with those of other Fe(III) heme proteins bearing cysteine(thiolate) coordinated opposite a neutral sixth ligand. A second, minor EPR signal with a narrower *g* anisotropy is observed in Fe(III)BxRcoM-2 (Figure 2); this signal was not simulated due to the very low intensity and the extent of overlap with the major signal. The presence of dual signals in low-spin heme-thiolate proteins, which may be due to differences in protonation of the thiolate ligand (36), has been observed for both RrCooA (37) and hCBS (38). The *g* anisotropy in low-spin Fe(III) hemes correlates with the nature of the axial ligands, and the narrow separation of  $g_x$ ,  $g_y$ , and  $g_z$  provides definitive evidence of a thiolate ligand in Fe(III)BxRcoM-2 (Table 2 and references therein) (39). In contrast, low-spin, Fe(III) heme proteins bearing two neutral donors (i.e., bis-histidine) typically exhibit a rhombic spectrum in which the

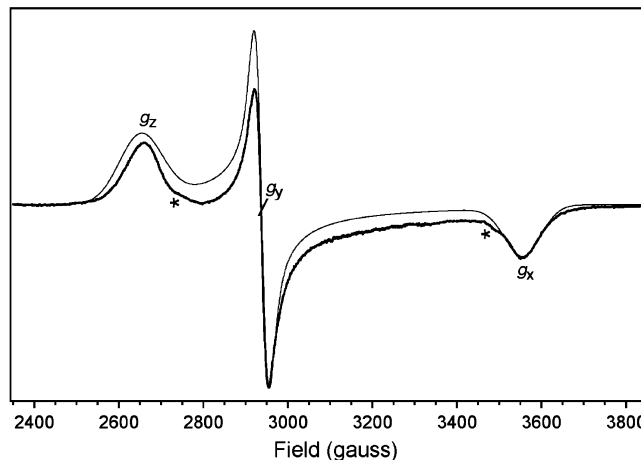


FIGURE 2: X-Band EPR spectrum of Fe(III)BxRcoM-2 (thick line) and best-fit simulation (thin line). The sample included 250  $\mu$ M heme in 50 mM borate buffer and 500 mM KCl (pH 8.0). The spectrum was recorded at 10 K with a 9.3567 GHz microwave frequency, a 0.505 mW microwave power, a  $3.2 \times 10^5$  receiver gain, an 8.31 G modulation amplitude, a 100 kHz modulation frequency, and a 163.84 ms time constant, using 10 added scans each containing 2048 data points. The background was corrected, and the best-fit simulation was generated. Asterisks denote the unsimulated minor second signal,  $g_x$  and  $g_z$  components.

Table 2: Comparison of EPR *g* Values for Selected Fe(III) Heme Proteins

protein	ligands	$g_z$	$g_y$	$g_x$	ref
BxRcoM-2 <sup>a</sup>	?/Cys	2.52	2.28	1.88	this work
RrCooA	Pro/Cys	2.46	2.25	1.89 (major)	37
RrCooA	Pro/Cys	2.58	2.25	1.84 (minor)	37
P450 <sub>CAM</sub> +ImH	ImH/Cys	2.56	2.27	1.87	55
hCBS	His/Cys	2.49	2.31	1.87 (major)	56
hCBS	His/Cys	2.43	2.31	1.90 (minor)	56
M80C cyt <i>c</i>	His/Cys	2.56	2.27	1.85	57
EcDos	His/H <sub>2</sub> O	3.42	—	—	76
cytochrome <i>b</i> <sub>5</sub>	His/His	3.03	2.23	1.43 (pH 7.0)	77
neuroglobin	His/His	3.14	2.16	1.34	78

<sup>a</sup> Experimental values.

*g* anisotropy is larger, e.g., cytochrome *b*<sub>5</sub> and neuroglobin. In cases where the axial ligands impose higher symmetry on the  $d_{xz}$  and  $d_{yz}$  iron orbitals, e.g., in EcDos, the unpaired electron becomes significantly delocalized, moving  $g_z$  ( $g_{\max}$ ) to a lower field while  $g_x$  and  $g_y$  become broad and nearly undetectable. Blumberg and Peisach (39) utilized the energy parameters *V* and  $\Delta$  as indicators of the strength and symmetry of the ligand field exerted by the axial ligands in low-spin Fe(III) hemes. Their analysis defined five regions in a crystal field diagram, which plotted the rhombic field (*V*/ $\Delta$ ) versus the tetragonal field ( $\Delta/\lambda$ ). Calculations using the *g* values measured for Fe(III)BxRcoM-2 yield field parameters that place BxRcoM-2 squarely within the “P” region of the Blumberg–Peisach diagram, which is populated by other cysteine(thiolate) Fe(III) heme proteins possessing a sixth neutral axial ligand.

Resonance Raman analysis of Fe(III)BxRcoM-2 (Figure 3B) identified vibrational modes associated with oxidation, spin and coordination states that are also consistent with a low-spin, six-coordinate Fe(III) heme. The high-frequency region of heme Raman spectra is dominated by porphyrin in-plane modes, which are sensitive to the heme iron oxidation state ( $\nu_4$ ) and spin and coordination states ( $\nu_3$ ,  $\nu_2$ , and  $\nu_{10}$ ) (33, 34). The Soret-excited resonance Raman

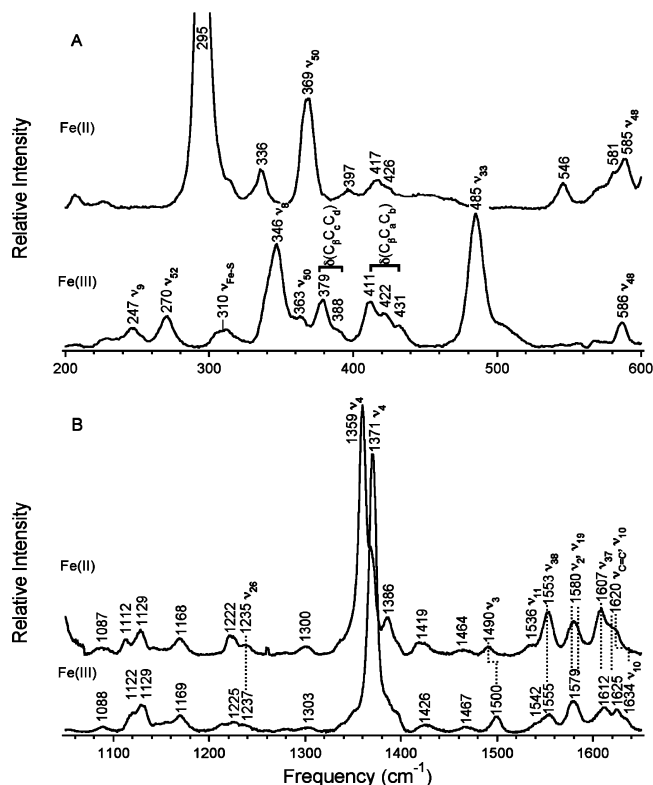


FIGURE 3: Resonance Raman spectra of Fe(III)*BxRcoM*-2 and Fe(II)*BxRcoM*-2. The sample included 250  $\mu$ M heme in 50 mM borate buffer and 500 mM KCl (pH 8.0). Reduction was performed using solid sodium dithionite. Spectra were recorded on the frozen samples at 77 K using the 413.1 nm Kr<sup>+</sup> laser line with a power of  $\sim$ 50 mW at the sample. Spectral windows are shown for (A) 200–600 and (B) 1050–1650  $\text{cm}^{-1}$  regions. Key vibrational modes are indicated.

spectrum for Fe(III)*BxRcoM*-2, shown in Figure 3B, displays porphyrin skeletal modes at frequencies expected for a low-spin Fe(III) heme: 1371  $\text{cm}^{-1}$  ( $\nu_4$ ), 1500  $\text{cm}^{-1}$  ( $\nu_3$ ), 1579  $\text{cm}^{-1}$  ( $\nu_2$ ), and 1634  $\text{cm}^{-1}$  ( $\nu_{10}$ ). Fe(III) heme centers exhibit the oxidation state marker band  $\nu_4$  in the range of  $\sim$ 1370–1375  $\text{cm}^{-1}$ , and for low-spin hemes, the most distinct spin state marker band  $\nu_3$  occurs in the range of 1500–1510  $\text{cm}^{-1}$  (33, 34). In contrast, high-spin, five- and six-coordinate Fe(III) hemes exhibit  $\nu_3$  bands at 1490–1500 and 1475–1485  $\text{cm}^{-1}$ , respectively. Though the porphyrin skeletal modes are largely insensitive to the identity of the iron axial ligands, the low-frequency region (200–700  $\text{cm}^{-1}$ ) can be useful in assigning vibrations associated with specific metal–ligand bonds (40). In previous work, Champion, et al. (41) characterized substrate-bound cytochrome P450<sub>CAM</sub> isotopically labeled with  $^{34}\text{S}$  and  $^{57}\text{Fe}$  and identified the stretching mode for the iron–sulfur bond ( $\nu_{\text{Fe-S}}$ ) at 351  $\text{cm}^{-1}$  for the high-spin Fe(III) enzyme. In the six-coordinate, low-spin Fe(III) heme of hCBS, global  $^{34}\text{S}$  labeling was used to identify  $\nu_{\text{Fe-S}}$  as a lower-energy band at 312  $\text{cm}^{-1}$  (42). In Figure 3A, by analogy to the assignment in hCBS, we tentatively identify  $\nu_{\text{Fe-S}}$  as a broad band centered at  $\sim$ 310  $\text{cm}^{-1}$ ; however, definitive assignment of this mode cannot be made without isotopic labeling. The breadth of this  $\sim$ 310  $\text{cm}^{-1}$  band suggests that there may be overlap of two different bond vibrations or slightly different environments around the thiolate ligand.

**Characterization of Fe(II)*BxRcoM*-2.** Treatment of Fe(III)*BxRcoM*-2 with a reducing agent results in a new

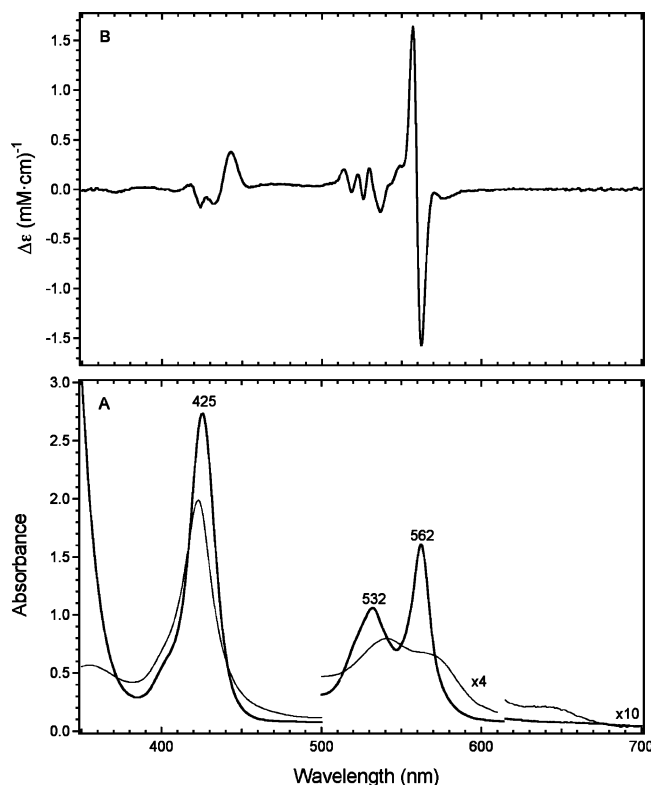


FIGURE 4: Electronic absorption (A) and MCD (B) spectra of Fe(II)*BxRcoM*-2. (A) The electronic absorption sample included 12  $\mu$ M heme in 25 mM EPPS buffer with 500 mM KCl (pH 8.0) at 25  $^{\circ}\text{C}$ . Sodium dithionite was added in slight excess as a solid to Fe(III)*BxRcoM*-2 (thin line) to prepare Fe(II)*BxRcoM*-2 (thick line). (B) The MCD sample included approximately 30  $\mu$ M heme in 25 mM EPPS buffer with 250 mM KCl (pH 8.0) and  $\sim$ 55% glycerol. The average of three scans collected at 4.5 K under a constant magnetic field (7 T) is shown.

electronic absorption spectrum suggestive of a low-spin, six-coordinate Fe(II) heme in which the cysteine(thiolate) ligand has been replaced. As shown in Figure 4A, when a reductant is added to Fe(III)*BxRcoM*-2, the Soret band maximum increases in intensity and red shifts slightly from 423 to 425 nm with simultaneous sharpening of the  $\alpha$  and  $\beta$  peaks, which shift to 562 and 532 nm, respectively (Figure 4A). Comparison of the spectral peak positions for Fe(II)*BxRcoM*-2 (Table 3 and references therein) with those of other heme proteins such as *RrCooA*, which undergo a ligand switch upon reduction, strongly suggests analogous behavior for *BxRcoM*-2. If cysteine(thiolate) were retained as an axial ligand after reduction of Fe(III)*BxRcoM*-2, the Soret maximum would be expected to appear at  $\sim$ 450 nm, as seen in reduced hCBS at pH 9. This is clearly not the case: the Soret maximum of Fe(II)*BxRcoM*-2 at 425 nm in Figure 4A shows conclusively that cysteine(thiolate) is replaced as an axial ligand. In the case of Fe(II)*CooA*, cysteine(thiolate) is replaced with a histidine; this change in coordination results in a Soret maximum with a peak position identical to that of Fe(II)*BxRcoM*-2 (425 nm), though the  $\alpha$  and  $\beta$  positions of Fe(II)*CooA* are both blue-shifted 3 nm relative to those of Fe(II)*BxRcoM*-2. Cytochrome *b*<sub>5</sub> and neuroglobin, which possess bis-histidine coordination in the Fe(II) state, also exhibit Soret positions similar to those of Fe(II)*BxRcoM*-2 and Fe(II)*CooA* (Table 3), supporting an assignment in Fe(II)*BxRcoM*-2 of two neutral donor axial ligands. When  $\alpha$  and  $\beta$  peak positions are considered, the observed spectral

Table 3: Comparison of Electronic Absorption and MCD Peak Positions for Selected Six-Coordinate Fe(II) Heme Proteins

protein	ligands	Soret	$\beta$	$\alpha$	ref			
Electronic Absorption								
<i>BxRcoM-2<sup>a</sup></i>	??	425	532	562	this work			
<i>RrCooA</i>	His/Pro	425	529	559	58			
hCBS (pH 9.0)	His/Cys	448	540	570	56			
cytochrome <i>c</i>	His/Met	413	521	550	79			
<i>EcDos</i>	His/Met	427	532	563	4			
cytochrome <i>b</i> <sub>5</sub>	His/His	423	526	556	80			
neuroglobin	His/His	426	530	560	59			
	Peak	Crossover	Peak	Peak	Crossover	Peak	ref.	
MCD								
<i>BxRcoM-2<sup>a</sup></i>	??	417	421	424	557	560	562	this work
<i>RrCooA</i>	His/Pro	416 <sup>b</sup>	420	425 <sup>b</sup>	550 <sup>b</sup>	554	558 <sup>b</sup>	81
hCBS (pH 9)	His/Cys	445 <sup>b</sup>	448	452 <sup>b</sup>	563 <sup>b</sup>	566	569 <sup>b</sup>	56
cytochrome <i>c</i>	His/Met	414	420	425	544 <sup>b</sup>	546	549 <sup>b</sup>	82
<i>EcDos</i>	His/Met	NR <sup>c</sup>	NR <sup>c</sup>	430	558	561	565	74
cytochrome <i>b</i> <sub>5</sub>	His/His	415	426	438	544	547	549	82
<sup>a</sup> Experimental values. <sup>b</sup> Peak positions were not reported in the original paper and are presented from inspection of the data. <sup>c</sup> Not reported.								

<sup>a</sup> Experimental values. <sup>b</sup> Peak positions were not reported in the original paper and are presented from inspection of the data. <sup>c</sup> Not reported.

data for Fe(II)*BxRcoM-2* most closely resemble those of Fe(II)*EcDos* (4), which possesses a low-spin, six-coordinate Fe(II) heme with histidine and methionine as axial ligands.

MCD spectroscopy corroborates the assignment of the Fe(II)*BxRcoM-2* protein as a low-spin, six-coordinate Fe(II) heme with two neutral axial ligands. The MCD spectrum of Fe(II)*BxRcoM-2*, shown in Figure 4B, is dominated by an intense temperature-independent A term in the  $\alpha$ - $\beta$  region with a crossover at 560 nm. Another much less intense temperature-independent feature is observed in the Soret region with a crossover at 421 nm. The temperature independence of the MCD spectral features is consistent with an assignment of  $S = 0$ , low-spin, Fe(II) heme. The dominant A term in the  $\alpha$ - $\beta$  region, also simply termed the alpha ( $\alpha$ ) band, is typical of Fe(II), low-spin heme systems, and its position is diagnostic for the type of axial ligation present (Table 3 and references therein). When cysteine(thiolate) is retained as a ligand after reduction, the  $\alpha$  band crossover occurs between 562 and 576 nm, which can be observed for Fe(II)*CBS* at pH 9. When the sixth position is occupied by a neutral/non-thiolate ligand, the crossover position blue shifts to  $\sim$ 550–560 nm, as observed in the Fe(II) states of *RrCooA* and *EcDos*. The position of the  $\alpha$  band in Fe(II)*BxRcoM-2* (560 nm), then, is in agreement with previous observations for other low-spin, six-coordinate Fe(II) hemes (Table 3), which contain two neutral donor ligands.

The resonance Raman spectrum of Fe(II)*BxRcoM-2* (Figure 3B) shows oxidation, spin, and coordination state vibrational modes consistent with the assignment of a low-spin, six-coordinate heme. In the Fe(II) state, the heme axial ligands compete more effectively for the iron  $d_{\pi}$  orbitals, which results in lowered frequencies for the  $\pi$ -sensitive marker bands, of which  $\nu_{11}$  is considered the most sensitive (33, 34). Fe(II)*BxRcoM-2* (Figure 3B) exhibits an oxidation state ( $\nu_4$ ) band at 1359  $\text{cm}^{-1}$ , which is appropriately shifted to a frequency lower than that of Fe(III)*RcoM-2* ( $\nu_4$ , 1371  $\text{cm}^{-1}$ ). The shoulder on  $\nu_4$  at 1368  $\text{cm}^{-1}$  is attributed to a fraction of CO-bound protein that is present in the as-isolated protein (26). The spin and coordination state bands ( $\nu_3$  and  $\nu_2$ ) for Fe(II)*BxRcoM-2* occur at 1490 and 1580  $\text{cm}^{-1}$ , respectively. The 1490  $\text{cm}^{-1}$  position of the spin state

marker ( $\nu_3$ ) is indicative of a low-spin system and is at lower frequency than in Fe(III)*BxRcoM-2* (1500  $\text{cm}^{-1}$ ). Marker band  $\nu_2$ , which overlaps with  $\nu_{19}$ , is not shifted appreciably from its position in Fe(III)*BxRcoM-2*; however, in Fe(II)*BxRcoM-2*,  $\nu_{10}$  is observed to shift to a lower frequency ( $\sim$ 1620  $\text{cm}^{-1}$ ), underneath a band associated with the  $\nu_{\text{C}=\text{C}}$  porphyrin mode. The degree of overlap of  $\nu_{11}$  with  $\nu_{38}$  decreases as  $\nu_{11}$  shifts to a lower frequency upon reduction of Fe(III)*BxRcoM-2*, and this band is located at  $\sim$ 1536  $\text{cm}^{-1}$  in the Fe(II)*BxRcoM-2* spectrum. The positions of all key marker bands in Fe(II)*BxRcoM-2* (Figure 3B) agree with expected values for low-spin, six-coordinate Fe(II) heme proteins in which both ligands are neutral donors (33, 34). Importantly, these characteristic vibrational frequencies are not consistent with either a high-spin state or the presence of cysteine(thiolate) as a heme iron ligand (43).

*Characterization of the Fe(II)CO Adduct of BxRcoM-2.* Electronic absorption and MCD spectra of Fe(II)CO *BxRcoM-2* (Figure 5) exhibit features consistent with the formation of a six-coordinate Fe(II)CO adduct with CO bound opposite a neutral ligand. In the presence of CO and reductant, the optical spectrum (Figure 5A) displays a slightly blue-shifted, very sharp, and intense Soret feature at 423 nm. The sharp, inequivalent  $\alpha$  and  $\beta$  peaks present in the Fe(II)*BxRcoM-2* spectrum are converted to a pair of nearly equivalent peaks at  $\sim$ 540 and 570 nm, respectively. The order of CO addition and reduction does not appreciably influence the peak intensity ratio in the visible region. The same spectrum is obtained either when CO(g) is added to Fe(II)*BxRcoM-2* or when dithionite is added to Fe(III)-*BxRcoM-2* in the presence of excess CO(g) (Figure 5A). The positions and shapes of the observed peaks in the UV and visible regions are typical for low-spin, six-coordinate Fe(II)CO heme adducts (Supporting Information, Table S2) in which CO binds opposite a neutral donor ligand. At 100 K, the MCD spectrum of Fe(II)CO *BxRcoM-2* (Figure 5B) is dominated by a derivative-shaped, temperature-independent A term in the Soret region with a crossover at 423 nm and another temperature-independent feature in the  $\alpha$ - $\beta$  region with a crossover at 571 nm. At temperatures normally used in low-temperature MCD (2–25 K), the CO adduct was susceptible to photolysis, which has been documented

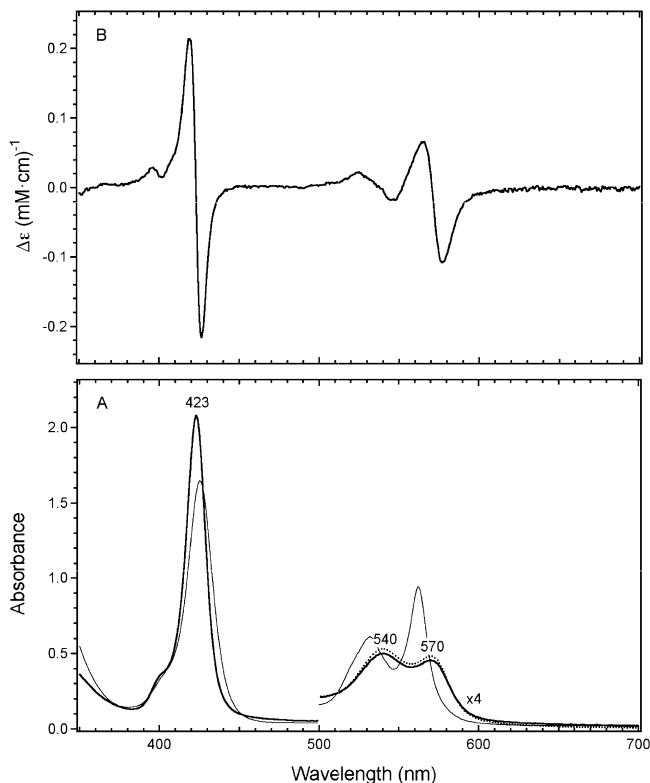


FIGURE 5: Electronic absorption (A) and MCD (B) spectra of Fe(II)CO *BxRcoM-2*. (A) Electronic absorption spectra of Fe(II)CO *BxRcoM-2*, with order of addition effects, are shown. A sample ( $\sim 8 \mu\text{M}$  heme) with CO<sub>(g)</sub> present at the time of reduction (solid line) is compared with a sample ( $\sim 8 \mu\text{M}$  heme) with CO<sub>(g)</sub> injected after reduction (dashed line). The Fe(II) Soret is shown (thin line); the Fe(II)CO Soret is the same in both experiments. (B) The MCD sample included  $\sim 30 \mu\text{M}$  heme in 25 mM EPPS buffer with 250 mM KCl (pH 8.0) and  $\sim 55\%$  glycerol. The average of three scans collected at 7 T and 100 K is shown. Samples were prepared in 25 mM EPPS buffer with 500 mM KCl (pH 8.0) maintained at 25 °C. A sodium dithionite solution was used to reduce the protein samples in panels A and B. For MCD (B), CO<sub>(g)</sub> was mixed with the Fe(III)*BxRcoM-2* sample before reduction.

for other six-coordinate CO-bound heme proteins (44). Comparison of the MCD peak positions (Supporting Information, Table S2) with those of other six-coordinate Fe(II)CO proteins shows a clear resemblance of Fe(II)CO *BxRcoM-2* to proteins with histidine as the axial ligand *trans* to CO.

Further characterization of Fe(II)CO *BxRcoM-2* utilized isotope-edited resonance Raman spectroscopy, as shown in Figure 6, to identify the Fe–CO and C–O stretching and bending modes to confirm the assignment of a six-coordinate CO adduct with a *trans* histidine ligand. The binding of CO, a  $\pi$  acid ligand, to the Fe(II) heme is expected to compete with the porphyrin macrocycle for iron  $d_{\pi}$  electrons, resulting in upshifts of  $\pi$ -sensitive marker bands toward Fe(III) frequencies as the porphyrin bonding modes strengthen. In Figure 6B, the marker bands that are sensitive to the Fe(II)CO oxidation, spin, and coordination states,  $\nu_4$  (1368 cm<sup>-1</sup>),  $\nu_2$  (1575 cm<sup>-1</sup>),  $\nu_3$  (1494 cm<sup>-1</sup>), and  $\nu_{10}$  (1630 cm<sup>-1</sup>), are observed to shift relative to those of the Fe(II)*BxRcoM-2* spectrum. The frequencies of the major observed bands in Fe(II)CO *BxRcoM-2* (Figure 6B) are in agreement with those of other six-coordinate CO–heme adducts with histidine as a *trans* ligand (45). Isotopic substitution with <sup>13</sup>CO identified the CO-associated stretching and bending modes, as shown

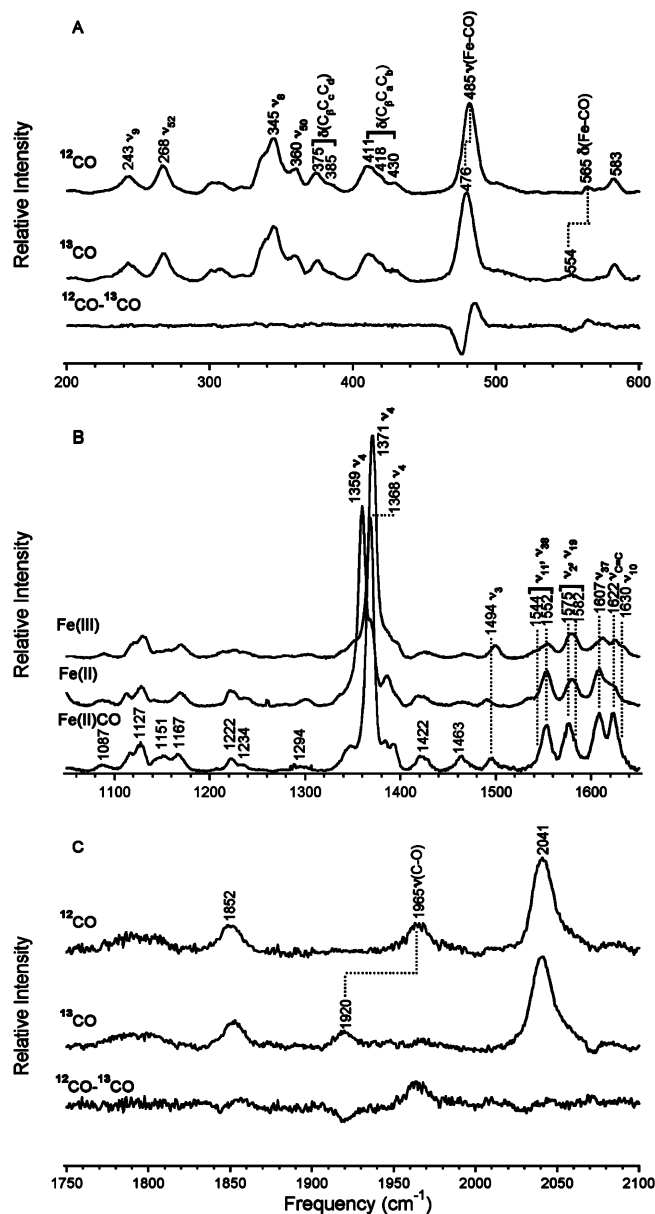


FIGURE 6: Resonance Raman spectra for Fe(II)(<sup>12</sup>CO) and Fe(II)(<sup>13</sup>CO) *BxRcoM-2*. The samples included 250  $\mu\text{M}$  heme in 50 mM borate buffer and 500 mM KCl (pH 8.0). After CO<sub>(g)</sub> was injected into the Fe(III)*BxRcoM-2* sample headspace, reduction was performed using a sodium dithionite solution. Spectra were of frozen samples were recorded at 77 K using the 413.1 nm Kr<sup>+</sup> laser line with an  $\sim 7$ –10 mW power at the sample. The difference spectrum (<sup>12</sup>CO – <sup>13</sup>CO) is shown for the frequency ranges containing  $\nu(\text{Fe–CO})$ ,  $\delta(\text{Fe–CO})$ , and  $\nu(\text{C–O})$ . (A) Lowest-frequency window, 200–600 cm<sup>-1</sup>, containing stretching and bending modes  $\nu(\text{Fe–CO})$  and  $\delta(\text{Fe–CO})$ . (B) Midfrequency window, 1050–1650 cm<sup>-1</sup>, containing the major oxidation, spin, and coordination state marker bands. Shown is a comparison of the Fe(III), Fe(II), and Fe(II)CO states. (C) High-frequency window, 1750–2100 cm<sup>-1</sup>, containing stretching mode  $\nu(\text{C–O})$ . Key vibrational modes are indicated.

in Figure 6A. The stretching modes [ $\nu(\text{Fe–}^{12}\text{CO})$ , 485 cm<sup>-1</sup>;  $\nu(\text{Fe–}^{13}\text{CO})$ , 476 cm<sup>-1</sup>] and bending modes [ $\delta(\text{Fe–}^{12}\text{CO})$ , 565 cm<sup>-1</sup>;  $\delta(\text{Fe–}^{13}\text{CO})$ , 554 cm<sup>-1</sup>] correlate well with those of known six-coordinate Fe(II)CO proteins (Supporting Information, Table S3 and references therein). In the high-frequency region, modes for the coordinated C–O stretches [ $\nu(^{12}\text{C–O})$ , 1965 cm<sup>-1</sup>;  $\nu(^{13}\text{C–O})$ , 1920 cm<sup>-1</sup>] are also observed (Figure 6C). The Fe–CO and internal C–O



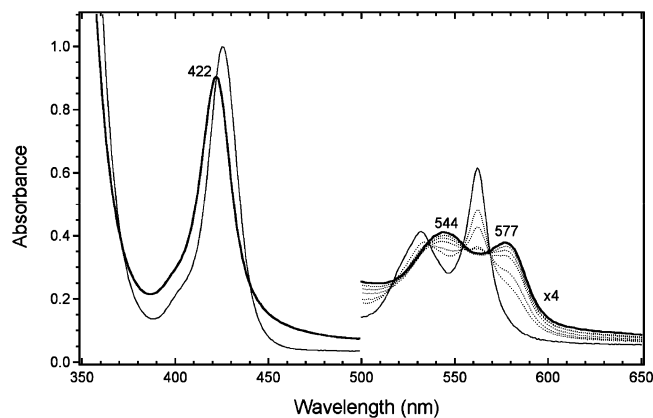


FIGURE 7: Electronic absorption spectrum of Fe(II)NO *BxRcoM-2*. The electronic absorption spectrum of Fe(II)NO *BxRcoM-2* (thick line) is shown overlaid on the Fe(II) spectrum (thin line). The conversion profile from the ferrous protein after a bolus of NO<sub>(g)</sub> was added is indicated in the  $\alpha$ - $\beta$  region (dotted line). The sample included 6  $\mu$ M heme in 25 mM EPPS buffer with 500 mM KCl (pH 8.0) maintained at 25 °C. The sample was prepared by reducing Fe(III)*BxRcoM-2* with solid sodium dithionite followed by addition of NO<sub>(g)</sub>.

stretching frequencies are linearly correlated with a negative coefficient; the ligand *trans* to CO also influences the observed frequencies of the two stretching modes (46, 47). When the protein environment surrounding CO becomes more positive,  $\pi$ -electrons are more highly delocalized from the Fe(II) to CO, strengthening the Fe–C bond, but weakening the C–O bond through increased population of the  $\pi^*$ -antibonding orbitals. The inverse is observed when the environment of the CO is more negative in nature. When the frequencies of the Fe–CO and C–O stretching modes are plotted on a  $\nu(\text{Fe–CO})/\nu(\text{C–O})$  correlation diagram (Supporting Information, Figure S2), the values for *BxRcoM-2* are observed to fall near a cluster of values for other six-coordinate Fe(II)CO heme proteins and related model complexes with histidine *trans* to CO. Furthermore, the position of Fe(II)CO *BxRcoM-2* on this correlation is consistent with a CO ligand which resides in a neutral, nonpolar environment.

**Characterization of the Fe(II)NO Adduct of *BxRcoM-2*.** Electronic absorption spectroscopy of Fe(II)NO *BxRcoM-2* reveals spectral features (Figure 7) characteristic of a six-coordinate Fe(II)NO heme. As illustrated in Figure 7, upon addition of NO<sub>(g)</sub>, the Soret absorption maximum of Fe(II)*BxRcoM-2* undergoes a blue shift from 425 nm to a slightly less intense, sharp Soret maximum at 422 nm, the shape and position of which are comparable to those of known six-coordinate Fe(II)NO heme proteins (Supporting Information, Table S4). The transition of the  $\alpha$  and  $\beta$  bands from the sharp, inequivalent peaks of the Fe(II) protein to the broader, more equivalent peaks at  $\sim$ 544 and 577 nm of the NO adduct is observed over several minutes (Figure 7) after a bolus of NO<sub>(g)</sub> is injected into the cuvette headspace. Five-coordinate NO–heme adducts, in which both endogenous ligands to iron have been displaced, display a broad, low-intensity blue-shifted Soret typically at  $\sim$ 400 nm with  $\alpha$  and  $\beta$  bands of approximately equivalent intensity (48). In contrast, six-coordinate NO–heme adducts, in which one endogenous ligand is retained opposite the NO, have distinct, sharp Soret bands with maxima in the range of 415–425 nm (49). The shape and position of the observed Fe(II)NO

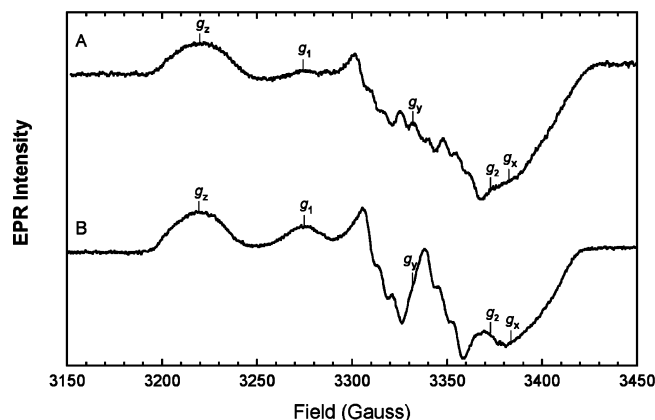


FIGURE 8: X-Band EPR spectra of (A) Fe(II)(<sup>14</sup>NO) and (B) Fe(II)(<sup>15</sup>NO) *BxRcoM-2*. Each sample included approximately 200  $\mu$ M heme in 50 mM borate buffer with 500 mM KCl (pH 8.0). The samples were prepared via reduction of Fe(III)*BxRcoM-2* followed by generation of NO<sub>(g)</sub>. Spectra were recorded at 10 K with a 9.3567 GHz microwave frequency, a 0.16 mW microwave power, a  $6.3 \times 10^5$  receiver gain, a 2.09 G modulation amplitude, a 100 kHz modulation frequency, and a 163.84 ms time constant, using 10 added scans containing 2048 data points.

Soret feature for *BxRcoM-2* in Figure 7 are clearly indicative of a six-coordinate heme. Nitric oxide is also able to bind to Fe(III) hemes and induce reduction of heme to Fe(II) (50). In the case of *BxRcoM-2*, the six-coordinate Fe(II)NO adduct forms readily over 5–10 min after NO<sub>(g)</sub> is introduced into an anaerobic Fe(III)*BxRcoM-2* sample (data not shown). Anaerobic samples of Fe(II)CO *BxRcoM-2*, however, remain relatively resistant to changes in coordination, even in the presence of a large excess of NO<sub>(g)</sub> (data not shown).

EPR spectroscopy of Fe(II)NO *BxRcoM-2* provides unambiguous confirmation of a six-coordinate Fe(II) heme in which NO binds opposite a nitrogen-containing endogenous protein ligand. The observed rhombic spectrum for the <sup>14</sup>NO adduct of Fe(II)*BxRcoM-2*, shown in Figure 8A, yields *g* values of 1.976, 2.005, and 2.076 for *g<sub>x</sub>*, *g<sub>y</sub>*, and *g<sub>z</sub>*, respectively. The presence of a sixth nitrogen-containing ligand opposite the bound <sup>14</sup>NO gives rise to a rhombic splitting pattern in which nine lines are observed due to hyperfine and superhyperfine coupling between the unpaired electron on the nitrogen of the NO ligand and the proximal ligand nitrogen atom (51). In Fe(II)(<sup>14</sup>NO) *BxRcoM-2*, the observed hyperfine and superhyperfine coupling constants are measured at  $\sim$ 22.5 and  $\sim$ 7.5 Gauss, respectively. The observed *g* values and coupling constants for the Fe(II)(<sup>14</sup>NO) adduct are similar to those of other six-coordinate Fe(II)NO heme proteins (Supporting Information, Table S5 and references therein). When isotopic substitution with <sup>15</sup>NO is performed (Figure 8B), hyperfine coupling of the unpaired electron with the  $I = 1/2$  <sup>15</sup>N nucleus results in the expected shift to a six-line spectrum with an increase in the hyperfine coupling constant to  $\sim$ 32.5 G and a slight decrease in the superhyperfine coupling constant to  $\sim$ 6.5 G; the *g* values remain consistent with those of Fe(II)(<sup>14</sup>NO) *BxRcoM-2*. These signals are clearly distinct from those of five-coordinate NO–heme adducts, which exhibit axially symmetric three-line spectra due to coupling of the electron with the single  $I = 1$  <sup>14</sup>N nucleus of the bound NO; isotopically substituted five-coordinate NO adducts have a hyperfine doublet due to the  $I = 1/2$  <sup>15</sup>N nucleus (51). The observed EPR spectra (Figure 8, both isotopomers) of Fe(II)-



NO *BxRcoM*-2 contain an additional feature at  $g_1 \sim 2.04$  with a complementary feature presumed to occur near  $g_2 \sim 1.98$ , which was not resolved in these spectra. These features are found in other six-coordinate Fe(II)NO adducts; the additional signals are attributed to alternate His–Fe(II)–NO structures, which vary in Fe(II)–His and Fe(II)–NO distances and in the Fe(II)–N–O angle (52).

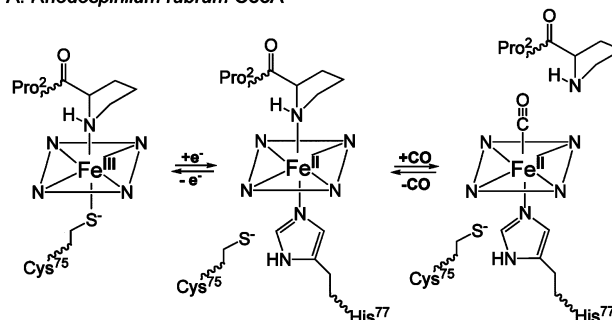
The assignment of a six-coordinate Fe(II)NO *BxRcoM*-2 adduct is also supported by resonance Raman data, which are shown in Figure S3 of the Supporting Information. Modes sensitive to the Fe(II)NO oxidation, spin, and coordination states,  $\nu_4$  ( $1371\text{ cm}^{-1}$ ),  $\nu_2$  ( $1575\text{ cm}^{-1}$ ),  $\nu_3$  ( $1496\text{ cm}^{-1}$ ), and  $\nu_{10}$  ( $1630\text{ cm}^{-1}$ ) (Supporting Information, Figure S3B), are in agreement with those of other six-coordinate Fe(II)NO heme proteins; no additional features were observed for  $\nu_3$  to indicate the presence of five-coordinate Fe(II)NO (53). In the low-frequency region, isotopic substitution with  $^{15}\text{NO}$  resolved a weak  $\nu(\text{Fe}–\text{NO})$  stretching mode [ $\nu(\text{Fe}–^{14}\text{NO})$ ,  $565\text{ cm}^{-1}$ ;  $\nu(\text{Fe}–^{15}\text{NO})$ ,  $552\text{ cm}^{-1}$ ] (Supporting Information, Figure S3A). Isotopic substitution with  $^{15}\text{NO}$  also results in the loss of a shoulder overlapping with  $\nu_{10}$ , which we tentatively assign as the  $\nu(^{14}\text{N}–\text{O})$  band at  $1631\text{ cm}^{-1}$  (Supporting Information, Figure S3C). The  $\nu(^{15}\text{N}–\text{O})$  stretching mode, which would be expected at  $\sim 1600–1605\text{ cm}^{-1}$ , was obscured by porphyrin skeletal modes with excitation at 413.1, 406.7, and 530 nm and cannot be assigned. The  $\nu(\text{Fe}–^{14}\text{NO})$  and tentative  $\nu(^{14}\text{N}–\text{O})$  frequencies correlate well with those of other six-coordinate Fe(II)NO proteins with histidine *trans* to NO (Supporting Information, Table S6). As with heme–CO adducts, the  $\nu(\text{Fe}–\text{NO})$  and  $\nu(\text{N}–\text{O})$  frequencies for proteins and model complexes are correlated; Fe(II)NO adducts follow a less well-behaved “anticorrelation” relationship (46). When the frequencies of  $\nu(\text{Fe}–\text{NO})$  and  $\nu(\text{N}–\text{O})$  for Fe(II)NO *BxRcoM*-2 are plotted (Supporting Information, Figure S4) with available protein and model complex data, the values of Fe(II)NO *BxRcoM*-2 fall near values for other six-coordinate Fe(II)NO heme proteins and related model complexes with a neutral/histidine ligand *trans* to NO.

## DISCUSSION

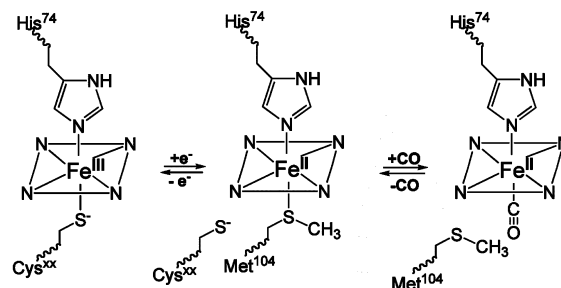
Functional studies of *BxRcoM*-1 and *BxRcoM*-2 implicate these proteins in aerobic CO sensing (26). The *rcoM* genes reside adjacent to open reading frames encoding aerobic CO-oxidizing machinery, and in *in vivo* reporter assays, both *BxRcoM* proteins drive CO-dependent transcription. Furthermore, in several organisms that lack a *cooA* gene, *rcoM* is found adjacent to the *coo* operon. These observations strongly suggest that RcoM serves as a CO-sensing transcription factor analogous to CooA. However, the *BxRcoM* proteins, with a heme-PAS domain and a LytR DNA-binding domain, are unrelated to CooA and utilize different heme coordination changes to transmit the CO signal. Our data suggest that the *B. xenovorans* RcoM proteins are also members of a more select group of heme-thiolate CO and NO gas-sensing proteins, which possess heme axial ligand environments that attenuate their sensing response to exclude regulation by  $\text{O}_2$ . As previously observed in *RrCooA* (6), the *BxRcoM*-2 heme appears to be tuned to sense CO as an effector ligand using a low-spin, six-coordinate heme environment and a redox-dependent ligand switch (Scheme 1).

Scheme 1: Heme Coordination Environments of (A) *RrCooA*, (B) *BxRcoM*,<sup>a</sup> and (C) *EcDos*

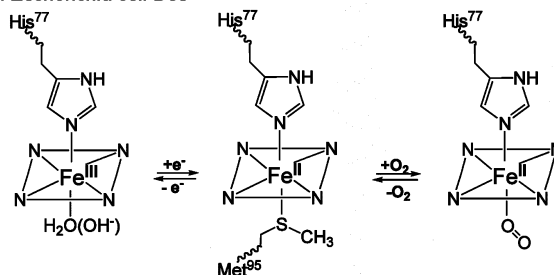
### A. *Rhodospirillum rubrum* CooA



### B. *Burkholderia xenovorans* RcoM



### C. *Escherichia coli* Dos



<sup>a</sup> The essential features of the *BxRcoM* redox and gas binding mechanism (B) include (1) a common histidine ligand in all states, (2) coordination of cysteine(thiolate) to Fe(III), (3) coordination of methionine to Fe(II), and (4) selective replacement of methionine with CO.

*BxRcoM*-2 exhibits striking spectral similarities to other members of the heme-thiolate family of gas-sensing proteins, including the heme-PAS sensor NPAS2. Resonance Raman and mutagenesis studies were used to identify the Fe(III) heme axial ligands of the NPAS2 PAS-A heme domain as Cys<sup>170</sup> and His<sup>119</sup> (54). Spectral comparisons of *BxRcoM*-2 to *RrCooA* (37), NPAS-2 (54), and other proteins with a neutral ligand opposite cysteine(thiolate) (55–57) suggest that a comparable coordination environment is present in *BxRcoM*-2. For example, the narrow  $g$  anisotropy characteristic of heme-thiolate proteins that is observed for Fe(III)*BxRcoM*-2 is similar to that seen for *RrCooA* (37). The thiolate-coordinated hemes of *BxRcoM*-2 and NPAS2 are distinct from those of the heme-containing PAS-domain proteins *EcDos*, *FixL*, and *AxPDEA1*. In both *FixL* and *AxPDEA1*, the Fe(III) heme is high-spin and five-coordinate, with a single conserved histidine ligand (3, 14). *EcDos*, in contrast, is low-spin and six-coordinate, with both the conserved histidine and a water (or hydroxide) coordinated to the heme iron (Scheme 1) (15).

Like *RrCooA* and NPAS2, *BxRcoM-2* undergoes a ligand switch when reduced, replacing the cysteine(thiolate) axial ligand, as illustrated in Scheme 1. All the spectral characteristics of Fe(II)*BxRcoM-2* are indicative of a low-spin, six-coordinate Fe(II) heme with two neutral donors, suggesting that the cysteine(thiolate) is no longer bound to the heme. Analogous replacement of a thiolate ligand upon reduction occurs in *RrCooA* (22, 23), where Cys<sup>75</sup> is replaced with His<sup>77</sup>, and in NPAS2, where Cys<sup>170</sup> is replaced with His<sup>171</sup> (54). In contrast, the O<sub>2</sub>-sensing PAS-domain proteins FixL and AxPDEA1 remain high-spin and five-coordinate in the reduced state (3, 14). Of the known gas-sensing heme-PAS domain proteins, only *EcDos* is low-spin and six-coordinate in both the Fe(III) and Fe(II) states; in the Fe(II) state, *EcDos* binds a methionine (Met<sup>95</sup>) opposite histidine, which replaces a coordinated water (15). Fe(III)*EcDos* and Fe(III)*BxRcoM-2* differ considerably in their spectral characteristics (Tables 1 and 2); however, there are considerable similarities between these proteins in their reduced states. Comparison of Fe(II)*EcDos* and Fe(II)*BxRcoM-2* leads to the interesting observation that, while the position of the Soret band in Fe(II)*BxRcoM-2* is most similar to those of proteins with two neutral nitrogen donors, i.e., *RrCooA* (58) and neuroglobin (59), the positions of the  $\alpha$  and  $\beta$  peaks are most similar to those of *EcDos* (4) (Table 3).

The identity of potential ligands in the *BxRcoM* proteins was inferred by sequence comparison among a related set of heme-PAS proteins and verified by mutational analysis (26). Alignment of the PAS domains of *BxRcoM-2*, its homologue *BxRcoM-1*, FixL proteins from two organisms, and *EcDos* suggested that His<sup>74</sup> in the *BxRcoM* proteins was a heme ligand candidate. Mutational analysis corroborated this proposal: in *BxRcoM-1*, alteration of His<sup>74</sup> eliminated accumulation of heme-bound protein. The spectral data for *BxRcoM-2* presented herein strongly suggest that histidine, presumably His<sup>74</sup>, is a ligand in both the Fe(III) and Fe(II) states. Our data further reveal that *BxRcoM-2* undergoes a redox-mediated ligand switch in which the cysteine(thiolate) ligand is replaced with a neutral donor. In the *BxRcoM* proteins, there are only three cysteines, Cys<sup>94</sup>, Cys<sup>127</sup>, and Cys<sup>130</sup>; studies are underway to identify which of these is the axial ligand to the Fe(III) heme. By analogy to *RrCooA* and NPAS2, we would expect a nearby neutral residue to replace cysteine in the Fe(II) state. A model for Fe(II) *BxRcoM-1*, using the structure of Fe(II)*EcDos* (17) as a template, placed either Met<sup>104</sup> or Met<sup>105</sup> in the proximity of the heme. Variants at Met<sup>104</sup>, but not Met<sup>105</sup>, altered *BxRcoM-1* visible spectral and functional behavior (26), consistent with the conclusion that Met<sup>104</sup> serves as a ligand to the Fe(II) heme. The observed spectroscopic data are consistent with, though not conclusive evidence for, the presence of the analogous Met<sup>104</sup> ligand in Fe(II)*BxRcoM-2*.

When Fe(II)*BxRcoM-2* binds CO, we infer that His<sup>74</sup> is retained as the sixth ligand, while Met<sup>104</sup> is replaced with CO (Scheme 1). The spectral features of Fe(II)CO *BxRcoM-2* in the electronic absorption, MCD, and resonance Raman spectra (Supporting Information, Table S2 and S3) are all consistent with the presence of histidine *trans* to CO. The observed Fe—CO and C—O stretching frequencies, when plotted on a correlation diagram (46), place *BxRcoM-2* on the correlation line for histidine as the *trans* ligand, near a

cluster of His/CO heme adducts that includes *EcDos* (Supporting Information, Figure S3). Furthermore, the correlation position indicates that the CO ligand is bound in a neutral/nonpolar environment in *BxRcoM-2* (45, 47), suggesting that the *BxRcoM-2* heme-PAS domain is comparable in hydrophobicity to those of FixL and *EcDos* (17, 60). In contrast, *RrCooA* has a C—O stretching frequency that is upshifted considerably (Supporting Information, Figure S3) (61).

Despite the strong negative *trans* influence of NO (62), which thermodynamically favors a five-coordinate NO—heme adduct, Fe(II)*BxRcoM-2* forms a six-coordinate nitrosyl adduct. EPR of the isotopically labeled <sup>14</sup>NO and <sup>15</sup>NO adducts reveals the presence of superhyperfine coupling that can arise only from the coordination of a nitrogen atom opposite the NO ligand at the heme iron. The most likely source of this nitrogen is His<sup>74</sup>, suggesting that Met<sup>104</sup> is the ligand that is replaced upon gas binding. The presence of a six-coordinate nitrosyl in the heme-PAS domain sensor proteins has precedent; the FixLs have been shown to form a temperature-dependent mixture of five- and six-coordinate NO adducts, and the six-coordinate NO adduct is favored by both AxPDEA1 and *EcDos* (63). Interestingly, in all heme-thiolate proteins thus far characterized, including *RrCooA* (58), hCBS (64), and NPAS2 (PAS-A) (54), coordination of NO to the heme iron causes the displacement of both axial ligands to form a five-coordinate NO adduct. Furthermore, the formation of the five-coordinate NO adduct in *RrCooA* results in inactivation of the protein, which implies that retention of the proximal histidine ligand is required for transcriptional activation in *RrCooA* (58). It is not yet clear what effect or relevance, if any, the binding of NO to form a six-coordinate adduct has on the DNA binding activity of *BxRcoM-1* or *BxRcoM-2*.

Patterns that illuminate how heme-based sensors discriminate among the three diatomic gases (O<sub>2</sub>, NO, and CO), which serve as signals in a variety of cellular systems, are now evident. In the O<sub>2</sub>-sensing PAS-domain proteins, as in hemoglobin and myoglobin, the Fe(II) heme is five-coordinate and high-spin, with a single histidine ligand (13, 65). The binding of O<sub>2</sub> to form a six-coordinate complex induces a spin state change, which alters local steric interactions and drives a global conformational change. In the FixL proteins, specificity for O<sub>2</sub> arises from interactions of the bound O<sub>2</sub> ligand with a conserved arginine residue via hydrogen bonding. Donation of a hydrogen bond to bound O<sub>2</sub>, as originally observed in the globins, appears to be a common selection mechanism for O<sub>2</sub>. In the H-NOX proteins, which are either O<sub>2</sub> or NO sensors, a distal pocket tyrosine is required to select for O<sub>2</sub> binding (66, 67). The tyrosine traps the bound O<sub>2</sub>, which would otherwise dissociate too rapidly to form a complex; H-NOX proteins without this tyrosine exhibit low affinities for O<sub>2</sub> and are NO sensors. *Trans* ligand influences amplify this discrimination: the O<sub>2</sub>-sensing proteins form a six-coordinate NO adduct, which is thermodynamically less favorable, while NO sensors form the thermodynamically preferred five-coordinate NO adduct. The H-NOX family member soluble guanylyl cyclase employs this strategy to bind NO with a high degree of discrimination against O<sub>2</sub> (68), and displacement of the *trans* histidine ligand to form the five-coordinate NO adduct induces enzyme activation (69). CO, which activates soluble guanylyl cyclase

only weakly, forms a six-coordinate adduct with retention of the histidine (68).

*RrCooA* uses this five- and six-coordination number difference to selectively respond to CO. *RrCooA* is active only when CO forms a six-coordinate adduct; the five-coordinate NO adduct is inactive for DNA binding (58). A *CooA* homologue from the thermophilic bacterium *C. hydrogenoformans* (*ChCooA*) forms six-coordinate NO and CO adducts at room temperature, both of which are active for DNA binding (70). At temperatures relevant to the physiological environment of the bacterium, the six-coordinate NO adduct reversibly converts to a five-coordinate NO adduct, suggesting that CO is the physiologically relevant regulator. Further selectivity for CO arises from the unique coordination properties of *RrCooA* that preclude formation of an O<sub>2</sub> adduct. The Fe(II) protein is six-coordinate, and only the strongly binding ligands NO and CO are able to replace the endogenous proline ligand. Furthermore, ligand switching between the Fe(II) and Fe(III) states ensures that the heme is oxidized by O<sub>2</sub>, as the Fe(III) heme is stabilized by its cysteine(thiolate) ligand.

Our data support a mechanism in which the *BxRcoM* proteins utilize selective ligand replacement to respond to CO, as illustrated in Scheme 1. The heme environment of *BxRcoM-2* shares similarities with both *RrCooA* and the heme-PAS gas sensor *EcDos*. Similar to that of *RrCooA*, the Fe(III) heme of *BxRcoM-2* is six-coordinate and low-spin with a cysteine(thiolate) as one of the ligands, and this cysteine(thiolate) is lost upon reduction. Like *EcDos* (16, 17), the new ligand in the Fe(II) state of *BxRcoM-2* is likely to be methionine. *EcDos* is unique among the heme-PAS gas sensors in requiring the rupture of a heme iron–ligand bond to bind a gas molecule, and Met<sup>95</sup> is the ligand that is replaced when gases bind. In the FixLs, A<sub>x</sub>PDEA1, and *EcDos*, a conserved arginine provides important hydrogen bonding contacts when O<sub>2</sub> binds (12); this residue is not conserved in the *BxRcoM* proteins (26). The absence of this key O<sub>2</sub> interaction in the *BxRcoM*s is consistent with a role in CO sensing. In *BxRcoM-2*, as in *EcDos*, the methionine ligand is more weakly bound than the histidine ligand, and therefore, it is the methionine that is selectively replaced upon effector binding. This ligand replacement is similar to that of *RrCooA*, in which the more weakly bound proline ligand is selectively replaced upon binding of CO (21, 71).

## CONCLUSION

Previous work by Kerby, et al. (26) and the work described herein demonstrate that *BxRcoM-2* and, by analogy, *BxRcoM-1* possess features similar to those of the well-characterized heme-thiolate CO-sensor *CooA* and the heme-PAS domain gas-sensing protein *EcDos*, which require the replacement of an endogenous ligand for gas binding. On the basis of the results of these studies, we propose that the resting state of Fe(III)*BxRcoM-2* is low-spin and six-coordinate with His<sup>74</sup>/Cys<sup>xx</sup> axially coordinated. Reduction results in the replacement of Cys<sup>xx</sup> with a nearby methionine (Met<sup>104</sup>), which is then itself replaced when CO binds opposite His<sup>74</sup>. Although replacement of His<sup>74</sup> with CO is plausible, Met<sup>104</sup> retention is not consistent with our observation that NO binds opposite an endogenous nitrogen-donor ligand. By analogy to other six-coordinate heme-based

sensors, *EcDos* and *RrCooA*, we propose that methionine serves in the *BxRcoM* proteins as a less avidly bound ligand, which is preferentially replaced by the CO effector molecule.

## ACKNOWLEDGMENT

We express thanks to Professor Thomas C. Brunold and his research group for their expertise and the generous use of their instrumentation. We also thank Dr. Frank Neese (MPI Mülheim, Mülheim, Germany) for the WEPR spectral fitting program.

## SUPPORTING INFORMATION AVAILABLE

Figures showing the MCD spectrum of Fe(III)*RcoM-2* (S1), the RR spectrum of Fe(II)NO *RcoM-2* (S3), and correlation plots of  $\nu(\text{Fe}–\text{CO})$  versus  $\nu(\text{C}–\text{O})$  (S2) and  $\nu(\text{Fe}–\text{NO})$  versus  $\nu(\text{N}–\text{O})$  (S4); parameters used to fit the EPR spectrum of Figure 2; and tables supporting the spectral interpretation (S1–S6). This material is available free of charge via the Internet at <http://pubs.acs.org>.

## REFERENCES

- Gilles-Gonzalez, M.-A., and Gonzalez, G. (2005) Heme-based sensors: Defining characteristics, recent developments, and regulatory hypotheses. *J. Inorg. Biochem.* 99, 1–22.
- Jain, R., and Chan, M. K. (2003) Mechanisms of ligand discrimination by heme proteins. *J. Biol. Inorg. Chem.* 8, 1–11.
- Gilles-Gonzalez, M. A., Gonzalez, G., Perutz, M. F., Kiger, L., Marden, M. C., and Poyart, C. (1994) Heme-based sensors, exemplified by the kinase FixL, are a new class of heme protein with distinctive ligand binding and autooxidation. *Biochemistry* 33, 8067–8073.
- Delgado-Nixon, V. M., Gonzalez, G., and Gilles-Gonzalez, M.-A. (2000) Dos, a heme-binding PAS protein from *Escherichia coli*, is a direct oxygen sensor. *Biochemistry* 39, 2685–2691.
- Hou, S., Larsen, R. W., Boudko, D., Riley, C. W., Karatan, E., Zimmer, M., Ordal, G. W., and Alam, M. (2000) Myoglobin-like aerotaxis transducers in archaea and bacteria. *Nature* 403, 540–544.
- Roberts, G. P., Kerby, R. L., Youn, H., and Conrad, M. (2005) CooA, a paradigm for gas sensing regulatory proteins. *J. Inorg. Biochem.* 99, 280–292.
- Dioum, E. M., Rutter, J., Tuckerman, J. R., Gonzalez, G., Gilles-Gonzalez, M.-A., and McKnight, S. L. (2002) NPAS2: A gas-responsive transcription factor. *Science* 298, 2385–2387.
- Arnold, W. P., Mittal, C. K., Katsuki, S., and Murad, F. (1977) Nitric oxide activates guanylate cyclase and increases guanosine 3',5'-cyclic monophosphate levels in various tissue preparations. *Proc. Natl. Acad. Sci. U.S.A.* 74, 3203–3207.
- Karow, D. S., Pan, D., Tran, R., Pellicena, P., Presley, A., Mathies, R. A., and Marletta, M. A. (2004) Spectroscopic characterization of the soluble guanylate cyclase-like heme domains from *Vibrio cholerae* and *Thermoanaerobacter tengcongensis*. *Biochemistry* 43, 10203–10211.
- Gu, Y. Z., Hogenesch, J. B., and Bradfield, C. A. (2000) The PAS superfamily: Sensors of environmental and developmental signals. *Annu. Rev. Pharmacol. Toxicol.* 40, 519–561.
- David, M., Daveran, M. L., Batut, J., Dedieu, A., Domergue, O., Ghai, J., Hertig, C., Boistard, P., and Kahn, D. (1988) Cascade regulation of *nif* gene expression in *Rhizobium meliloti*. *Cell* 54, 671–683.
- Dunham, C. M., Dioum, E. M., Tuckerman, J. R., Gonzalez, G., Scott, W. G., and Gilles-Gonzalez, M. A. (2003) A distal arginine in oxygen-sensing heme-PAS domains is essential to ligand binding, signal transduction, and structure. *Biochemistry* 42, 7701–7708.
- Tuckerman, J. R., Gonzalez, G., Dioum, E. M., and Gilles-Gonzalez, M. A. (2002) Ligand and oxidation-state specific regulation of the heme-based oxygen sensor FixL from *Sinorhizobium meliloti*. *Biochemistry* 41, 6170–6177.
- Chang, A. L., Tuckerman, J. R., Gonzalez, G., Mayer, R., Weinhouse, H., Volman, G., Amikam, D., Benziman, M., and Gilles-Gonzalez, M. A. (2001) Phosphodiesterase A1, a regulator



- of cellulose synthesis in *Acetobacter xylinum*, is a heme-based sensor. *Biochemistry* 40, 3420–3426.
15. Sasakura, Y., Yoshimura-Suzuki, T., Kurokawa, H., and Shimizu, T. (2006) Structure-function relationships of EcDOS, a heme-regulated phosphodiesterase from *Escherichia coli*. *Acc. Chem. Res.* 39, 37–43.
  16. Tanaka, A., Takahashi, H., and Shimizu, T. (2007) Critical role of the heme axial ligand, Met95, in locking catalysis of the phosphodiesterase from *Escherichia coli* (EcDOS) toward cyclic diGMP. *J. Biol. Chem.* 282, 21301–21307.
  17. Kurokawa, H., Lee, D. S., Watanabe, M., Sagami, I., Mikami, B., Raman, C. S., and Shimizu, T. (2004) A redox-controlled molecular switch revealed by the crystal structure of a bacterial heme PAS sensor. *J. Biol. Chem.* 279, 20186–20193.
  18. Reick, M., Garcia, J. A., Dudley, C., and Mcknight, S. L. (2001) NPAS2: An analog of clock operative in the mammalian forebrain. *Science* 293, 506–509.
  19. Aono, S. (2003) Biochemical and biophysical properties of the CO-sensing transcriptional activator CooA. *Acc. Chem. Res.* 36, 825–831.
  20. Lanzilotta, W. N., Schuller, D. J., Thorsteinsson, M. V., Kerby, R. L., Roberts, G. P., and Poulos, T. L. (2000) Structure of the CO-sensing transcription activator CooA. *Nat. Struct. Biol.* 7, 876–880.
  21. Clark, R. W., Youn, H., Parks, R. B., Cherney, M. M., Roberts, G. P., and Burstyn, J. N. (2004) Investigation of the role of the N-terminal proline, the distal ligand in the CO sensor CooA. *Biochemistry* 43, 14149–14160.
  22. Shelper, D., Thorsteinsson, M. V., Kerby, R. L., Chung, S.-Y., Roberts, G. P., Reynolds, M. F., Parks, R. B., and Burstyn, J. N. (1999) Identification of two important heme site residues (Cysteine 75 and Histidine 77) in CooA, the CO-sensing transcription factor of *Rhodospirillum rubrum*. *Biochemistry* 38, 2669–2678.
  23. Aono, S., Ohkubo, K., Matsuo, T., and Nakajima, H. (1998) Redox-controlled ligand exchange of the heme in the CO-sensing transcriptional activator CooA. *J. Biol. Chem.* 273, 25757–25764.
  24. Kerby, R. L., Youn, H., Thorsteinsson, M. V., and Roberts, G. P. (2003) Repositioning about the dimer interface of the transcription regulator CooA: A major signal transduction pathway between the effector and DNA-binding domains. *J. Mol. Biol.* 325, 809–823.
  25. Coyle, C. M., Puranik, M., Youn, H., Nielsen, S. B., Williams, R. D., Kerby, R. L., Roberts, G. P., and Spiro, T. G. (2003) Activation mechanism of the CO sensor CooA: Mutational and resonance Raman spectroscopic studies. *J. Biol. Chem.* 278, 35384–35393.
  26. Kerby, R. L., Youn, H., and Roberts, G. P. (2008) RcoM: A new single-component transcriptional regulator of CO metabolism in bacteria. *J. Bacteriol.* 190, 3336–3343.
  27. Chain, P. S. G., Denev, V. J., Konstantinidis, K. T., Vergez, L. M., Agullo, L., Reyes, V. L., Hauser, L., Cordova, M., Gomez, L., Gonzalez, M., Land, M., Lao, V., Larimer, F., Lipuma, J. J., Mahenthalingam, E., Malfatti, S. A., Marx, C. J., Parnell, J. J., Ramette, A., Richardson, P., Seeger, M., Smith, D., Spilker, T., Sul, W. J., Tsoi, T. V., Ulrich, L. E., Zhulin, I. B., and Tiedje, J. M. (2006) *Burkholderia xenovorans* LB400 harbors a multi-replicon, 9.73-Mbp genome shaped for versatility. *Proc. Natl. Acad. Sci. U.S.A.* 103, 15280–15287.
  28. Dykxhoorn, D. M., Pierre, R. S., and Linn, T. (1996) Synthesis of the end subunits of *Escherichia coli* RNA polymerase is autogenously regulated in vivo by both transcriptional and translational mechanisms. *Gene* 177, 133–136.
  29. Waterman, M. R. (1978) Spectral characterization of human hemoglobin and its derivatives. *Methods Enzymol.* 52, 456–463.
  30. Neese, F. (1997) Electronic structure and spectroscopy of novel copper chromophores in biology. Ph.D. Thesis, University of Konstanz, Konstanz, Germany.
  31. Abe, M., Kitagawa, T., and Kyogoku, Y. (1978) Resonance Raman spectra of octaethylporphyrinato-Ni(II) and meso-deuterated and <sup>15</sup>N substituted derivatives. II. A normal coordinate analysis. *J. Chem. Phys.* 69, 4526–4534.
  32. Woodruff, W. H., Adams, D. H., Spiro, T. G., and Yonetani, T. (1975) Resonance Raman spectra of cobalt myoglobins and cobalt porphyrins. Evaluation of protein effects on porphyrin structure. *J. Am. Chem. Soc.* 97, 1695–1698.
  33. Spiro, T. G. (1975) Resonance Raman spectroscopic studies of heme proteins. *Biochim. Biophys. Acta* 416, 169–189.
  34. Spiro, T. G., and Strekas, T. C. (1974) Resonance Raman spectra of heme proteins. Effects of oxidation and spin state. *J. Am. Chem. Soc.* 96, 338–345.
  35. Dawson, J. H., Andersson, L. A., and Sono, M. (1982) Spectroscopic investigations of ferric cytochrome P-450<sub>CAM</sub> ligand complexes. *J. Biol. Chem.* 257, 3606–3617.
  36. Pazicni, S. (2006) Towards understanding the role of the heme cofactor in cystathionine  $\beta$ -synthase. Ph.D. Thesis, University of Wisconsin, Madison, WI.
  37. Reynolds, M. F., Shelper, D., Kerby, R. L., Parks, R. B., Roberts, G. P., and Burstyn, J. N. (1998) EPR and electronic absorption spectroscopies of the CO-sensing CooA protein reveal a cysteine-ligated low-spin ferric heme. *J. Am. Chem. Soc.* 120, 9080–9081.
  38. Omura, T., Sadano, H., Hasegawa, T., Yoshida, Y., and Kominami, S. (1996) Hemoprotein H-450 identified as a form of cytochrome P-450 having an endogenous ligand at the 6th coordination position of the heme. *J. Biochem.* 96, 1491–1500.
  39. Blumberg, W. E., and Peisach, J. (1971) Low-spin compounds of heme proteins. *Adv. Chem. Ser.* 100, 271–291.
  40. Desbois, A., Lutz, M., and Banerjee, R. (1979) Low-frequency vibrations in resonance Raman spectra of horse heart myoglobin. Iron-ligand and iron-nitrogen vibration models. *Biochemistry* 18, 1510–1518.
  41. Champion, P. M., Stallard, B. R., Wagner, G. C., and Gunsalus, I. C. (1982) Resonance Raman detection of an Fe-S bond in cytochrome P450<sub>CAM</sub>. *J. Am. Chem. Soc.* 104, 5469–5472.
  42. Green, E. L., Taoka, S., Banerjee, R., and Loehr, T. M. (2001) Resonance Raman characterization of the heme cofactor in cystathionine  $\beta$ -synthase. Identification of the Fe-S(Cys) vibration in the six-coordinate low-spin heme. *Biochemistry* 40, 459–463.
  43. Champion, P. M., Gunsalus, I. C., and Wagner, G. C. (1978) Resonance Raman investigations of cytochrome P450<sub>CAM</sub> from *Pseudomonas putida*. *J. Am. Chem. Soc.* 100, 3743–3751.
  44. Brittain, T., Greenwood, C., Springall, J., and Thomson, A. J. (1982) The nature of ferrous haem protein complexes prepared by photolysis. *Biochim. Biophys. Acta* 703, 117–128.
  45. Tsubaki, M., Srivastava, R. B., and Yu, N.-T. (1982) Resonance Raman investigation of carbon monoxide bonding in (carbonmonoxy)hemoglobin and -myoglobin: Detection of Fe-CO stretching and Fe-C-O bending vibrations and influence of quaternary structure change. *Biochemistry* 21, 1132–1140.
  46. Ibrahim, M., Xu, C., and Spiro, T. G. (2006) Differential sensing of protein influences by NO and CO vibrations in heme adducts. *J. Am. Chem. Soc.* 128, 16834–16845.
  47. Vogel, K. M., Kozlowski, P. M., Zgierski, M. Z., and Spiro, T. G. (1999) Determinants of the FeXO [X = C, N, O] vibrational frequencies in heme adducts from experiment and density functional theory. *J. Am. Chem. Soc.* 121, 9915–9921.
  48. Stone, J. R., Sands, R. H., Dunham, W. R., and Marletta, M. A. (1995) Electron paramagnetic resonance evidence for the formation of a pentacoordinate nitrosyl-heme complex in soluble guanylate cyclase. *Biochem. Biophys. Res. Commun.* 207, 572–577.
  49. Yoshimura, T., and Ozaki, T. (1984) Electronic spectra for nitrosyl(protoporphyrin IX dimethyl ester)iron(II) and its complexes with nitrogenous bases as model systems for nitrosylhemoproteins. *Arch. Biochem. Biophys.* 229, 126–135.
  50. Addison, A. W., and Stephanos, J. J. (1986) Nitrosyliron(III) hemoglobin: Autoreduction and spectroscopy. *Biochemistry* 25, 4104–4113.
  51. Palmer, G. (1983) Electron paramagnetic resonance of hemoproteins. In *Iron Porphyrins* (Lever, A. B. P., and Gray, H. B., Eds.) pp 43–88, Addison-Wesley, Reading, MA.
  52. Morse, R. H., and Chan, S. I. (1980) Electron paramagnetic resonance studies of nitrosyl ferrous heme complexes: Determination of an equilibrium between two conformations. *J. Biol. Chem.* 255, 7876–7882.
  53. Mackin, H. C., Benko, B., Yu, N. T., and Gersonde, K. (1983) Resonance Raman study on pentacoordinated and hexacoordinated ferrous nitrosyl myoglobin. The influence of pH. *FEBS Lett.* 158, 199–202.
  54. Uchida, T., Sato, E., Sato, A., Sagami, I., Shimizu, T., and Kitagawa, T. (2005) CO-dependent activity-controlling mechanism of heme-containing CO-sensor protein, neuronal PAS domain protein 2. *J. Biol. Chem.* 280, 21358–21368.
  55. Lipscomb, J. D. (1980) Electron paramagnetic resonance detectable states of cytochrome P-450<sub>CAM</sub>. *Biochemistry* 19, 3590–3599.
  56. Pazicni, S., Lukat-Rodgers, G. S., Oliveriusova, J., Rees, K. A., Parks, R. B., Clark, R. W., Rodgers, K. R., Kraus, J. P., and Burstyn, J. N. (2004) The redox behavior of the heme is cystathionine  $\beta$ -synthase is sensitive to pH. *Biochemistry* 43, 14684–14695.

57. Wuttke, D. S. (1993) Preparation, characterization and intramolecular electron transfer studies of ruthenium-modified cytochromes c, pp 408–413, Ph.D. Thesis, California Institute of Technology, Pasadena, CA.
58. Reynolds, M. F., Parks, R. B., Burstyn, J. N., Shelper, D., Thorsteinsson, M. V., Kerby, R. L., Roberts, G. P., Vogel, K. M., and Spiro, T. G. (2000) Electronic absorption, EPR and resonance Raman spectroscopies of CooA, a CO-sensing transcription factor from *R. rubrum*, reveals a five-coordinate NO-heme. *Biochemistry* 39, 388–396.
59. Dewilde, S., Kiger, L., Burmester, T., Hankeln, T., Baudin-Creuz, V., Aerts, T., Marden, M. C., Caubergs, R., and Moens, L. (2001) Biochemical characterization and ligand binding properties of neuroglobin, a novel member of the globin family. *J. Biol. Chem.* 276, 38949–38955.
60. Key, J., and Moffat, K. (2005) Crystal structure of deoxy and CO-bound B<sub>j</sub>FixLH reveal details of ligand recognition and signaling. *Biochemistry* 44, 4627–4635.
61. Uchida, T., Ishikawa, H., Takahashi, S., Ishimori, K., Morishima, I., Ohkubo, K., Nakajima, H., and Aono, S. (1998) Heme environmental structure of CooA is modulated by the target DNA binding. Evidence from resonance Raman spectroscopy and CO rebinding kinetics. *J. Biol. Chem.* 273, 19988–19992.
62. Traylor, T. G., and Sharma, V. S. (1992) Why NO? *Biochemistry* 31, 2847–2849.
63. Tomita, T., Gonzalez, G., Chang, A. L., Ikeda-Saito, M., and Gilles-Gonzalez, M. A. (2002) A comparative resonance Raman analysis of heme-binding PAS domains: Heme iron coordination structures of the B<sub>j</sub>FixL, A<sub>x</sub>PDEA1, EcDos, and MtDos proteins. *Biochemistry* 41, 4819–4826.
64. Taoka, S., and Banerjee, R. (2001) Characterization of NO binding to human cystathionine  $\beta$ -synthase: Possible implications of the effects of CO and NO binding to the human enzyme. *J. Inorg. Biochem.* 87, 245–251.
65. Hao, B., Isaza, C., Arndt, J., Soltis, M., and Chan, M. K. (2002) Structure-based mechanism of O<sub>2</sub> sensing and ligand discrimination by the FixL heme domain of *Bradyrhizobium japonicum*. *Biochemistry* 41, 12952–12958.
66. Nioche, P., Berka, V., Vipond, J., Minton, N., Tsai, A.-L., and Raman, C. S. (2004) Femtomolar sensitivity of a NO sensor from *Clostridium botulinum*. *Science* 306, 1550–1553.
67. Boon, E. M., and Marletta, M. A. (2005) Ligand discrimination in soluble guanylate cyclase and the H-NOX family of heme sensor proteins. *Curr. Opin. Chem. Biol.* 9, 441–446.
68. Burstyn, J. N., Yu, A. E., Dierks, E. A., Hawkins, B. K., and Dawson, J. H. (1995) Studies of the heme coordination and ligand binding properties of soluble guanylyl cyclase(sGC): Characterization of Fe(II)sGC and Fe(II)sGC(CO) by electronic absorption and magnetic circular dichroism spectroscopies and failure of CO to activate the enzyme. *Biochemistry* 34, 5896–5903.
69. Dierks, E. A., and Burstyn, J. N. (1996) Nitric oxide (NO), the only nitrogen monoxide redox form capable of activating soluble guanylyl cyclase. *Biochem. Pharmacol.* 51, 1593–1600.
70. Clark, R. W., Lanz, N. D., Lee, A. J., Kerby, R. L., Roberts, G. P., and Burstyn, J. N. (2006) Unexpected NO-dependent DNA binding by the CooA homolog from *Carboxydotherrmus hydrogenoformans*. *Proc. Natl. Acad. Sci. U.S.A.* 103, 891–896.
71. Pinkert, J., Clark, R. W., and Burstyn, J. N. (2006) Modeling proline ligation in the heme-dependent CO sensor, CooA, using molecule analogs. *J. Biol. Inorg. Chem.* 5, 642–650.
72. Lu, Y., Casimiro, D. R., Bren, K. L., Richards, J. H., and Gray, H. B. (1993) Structurally engineered cytochromes with unusual ligand-binding properties: Expression of *Saccharomyces cerevisiae* Met-80-Ala iso-1-cytochrome c. *Proc. Natl. Acad. Sci. U.S.A.* 90, 11456–11459.
73. Banci, L., and Assfalg, M. (2001) Mitochondrial cytochrome c. In *Handbook of Metalloproteins* (Messerschmidt, A. H. R., Poulos, T., and Weighardt, K., Eds.) pp 33–43, John Wiley and Sons, Chichester, U.K.
74. Hirata, S., Matsui, T., Sasakura, Y., Sugiyama, S., Yoshimura, T., Sagami, I., and Shimizu, T. (2003) Characterization of Met95 mutants of a heme-regulated phosphodiesterase from *Escherichia coli*. Optical absorption, magnetic circular dichroism, circular dichroism, and redox potentials. *Eur. J. Biochem.* 270, 4771–4779.
75. Mathews, F. S. (2001) b-Type cytochrome electron carriers: Cytochromes b<sub>562</sub> and b<sub>5</sub>, and flavocytochrome b<sub>2</sub>. In *Handbook of Metalloproteins* (Messerschmidt, A. H. R., Poulos, T., and Weighardt, K., Eds.) pp 33–43, John Wiley and Sons, Chichester, U.K.
76. Gonzalez, G., Dioum, E. M., Bertolucci, C. M., Tomita, T., Ikeda-Saito, M., Cheesman, M. R., Watmough, N. J., and Gilles-Gonzalez, M.-A. (2002) Nature of the displaceable heme-axial residue in the EcDos protein, a heme-based sensor from *Escherichia coli*. *Biochemistry* 41, 8414–8421.
77. Boiss-Poltoratzsky, R., and Ehrenberg, A. (1967) Magnetic and spectrophotometric investigations of cytochrome b<sub>5</sub>. *Eur. J. Biochem.* 2, 361–365.
78. Nistor, S. V., Goovaerts, E., Van Doorslaer, S., Dewilde, S., and Moens, L. (2002) EPR-spectroscopic evidence of a dominant His–Fe III–His coordination in ferric neuroglobin. *Chem. Phys. Lett.* 361, 355–361.
79. Margoliash, E., and Frohwirt, N. (1959) Spectrum of horse-heart cytochrome c. *Biochem. J.* 71, 570–572.
80. Vickery, L., Salmon, A., and Sauer, K. (1975) Magnetic circular dichroism studies on microsomal aryl hydrocarbon hydroxylase: Comparison with cytochrome b<sub>5</sub> and cytochrome P-450<sub>CAM</sub>. *Biochim. Biophys. Acta* 386, 87–98.
81. Dhawan, I. K., Shelper, D., Thorsteinsson, M. V., Roberts, G. P., and Johnson, M. K. (1999) Probing the heme axial ligation in the CO-sensing CooA protein with magnetic circular dichroism spectroscopy. *Biochemistry* 38, 12805–12813.
82. Vickery, L., Nozawa, T., and Sauer, K. (1976) Magnetic circular dichroism studies of low-spin cytochromes. Temperature dependence and effects of axial coordination of the spectra of cytochrome c and cytochrome b<sub>5</sub>. *J. Am. Chem. Soc.* 98, 351–357.

BI800486X